arXiv:0706.0183v2 [nucl-th] 18 Sep 2007

Regge approach to charged-pion photoproduction at invariant energies above 2 GeV

A. Sibirtsev[1,2], J. Haidenbauer[3], S. Krewald[3], T.-S.H. Lee[1,4], U.-G. Meißner[2,3] and A.W. Thomas[1,5,6]

1 Excited Baryon Analysis Center (EBAC), Thomas Jefferson National Accelerator Facility, Newport News, Virginia 23606, USA
2 Helmholtz-Institut für Strahlen- und Kernphysik (Theorie), Universität Bonn, Nußallee 14-16, D-53115 Bonn, Germany
3 Institut für Kernphysik (Theorie), Forschungszentrum Jülich, D-52425 Jülich, Germany
4 Physics Division, Argonne National Laboratory, Argonne, Illinois, 60439, USA
5 Theory Center, Thomas Jefferson National Accelerator Facility, 12000 Jefferson Ave., Newport News, Virginia 23606, USA
6 College of William and Mary, Williamsburg, VA 23187, USA

Abstract. A Regge model with absorptive corrections is employed in a global analysis of the world data on positive and negative pion photoproduction for photon energies from 3 to 8 GeV. In this region resonance contributions are expected to be negligible so that the available experimental information on differential cross sections and single polarization observables at $-t{\leq}2$ GeV^2 allows us to determine the non-resonant part of the reaction amplitude reliably. The model amplitude is then used to predict observables for photon energies below 3 GeV. Differences between our predictions and data in this energy region are systematically examined as possible signals for the presence of excited baryons. We find that the data available for the polarized photon asymmetry show promising resonance signatures at invariant energies around 2 GeV. With regard to differential cross sections the analysis of negative pion photoproduction data, obtained recently at JLab, indicates likewise the presence of resonance structures around 2 GeV.

PACS. 11.55.Jy Regge formalism – 13.60.Le Meson production – 13.60.-r Photon and charged-lepton interactions with hadrons – 25.20.Lj Photoproduction reactions

1 Introduction

The generation of hadron mass including the excited baryon spectrum [1,2,3,4,5,6,7,8] is one of the unsolved puzzles of QCD that explicitly involves such fundamental properties as chiral symmetry and confinement. Historically, and on a more phenomenological level, there are two different approaches to hadron mass generation. The first, beginning with the Gell-Mann-Levy sigma model [9] and the Nambu-Jona-Lasino model [10] has the mass originating from the spontaneous breaking of chiral symmetry. An alternative approach considers mass generation in terms of the energy accumulation in the string connecting color charges, which results in the very successful phenomenology of Regge trajectories for high lying baryons [11, 12,13,14,15,16,17,18]. On a more fundamental level, the generation of mass in QCD is related to the anomalous breaking of the scale invariance of the classical gauge theory in terms of the trace anomaly [19,20]. This anomaly clearly shows that hadrons made of light quarks acquire the bulk of their mass from field (binding) energy.

A rough inspection of the excited baryon spectrum as given by the Particle Data Group [21] suggests an impressive regularity for nucleon and Delta states above $\simeq$1.8 GeV. The states with the same spin but opposite parity are almost degenerate. At the same time, a parity doubling is not observed for the well established low lying baryons. Unfortunately, the PDG has

only assigned many of these observed states one or two stars and some of the doublet partners for the baryons with masses above 2 GeV have not been observed because the spectroscopy of high lying baryons is a non-trivial problem. Therefore the crucial question of whether the parity doubling of the high mass baryons has systematic nature remains open.

Obviously, one can equally well ask why parity doubling was not observed for low mass baryons and what is the QCD symmetry behind this phenomenon? Only recently it was proposed [22,23,24,25,26,27,28,29,30] that parity doubling might reflect the restoration of spontaneously broken chiral symmetry of QCD. A clear testable prediction of chiral symmetry restoration is the existence of chiral partners of those high-lying states with a 4-stars rating[1], namely the $N(2190)$ and $N(2600)$. The parity partners of those established states are presently missing in the known baryon spectrum. Note that there are also missing chiral partners of N and Δ baryons, rated with less than three stars, in the mass region from 2.2 to 3 GeV as listed, for instance, in Ref. [31].

However, these speculations about chiral symmetry restoration in the spectrum are not the only way to explain the appar-

---

[1] The G_{17} baryon with mass of $\simeq$2.19 GeV and spin J=7/2 is quoted [21] with four stars and has negative parity. The $I_{1,11}$ has mass $\simeq$2.6 GeV, spin J=11/2, negative parity and is quoted with three stars.

ent doubling phenomenon. It was shown in the framework of a covariant constituent quark model [32,33], that the instanton induced multi-fermion interaction leads to a lowering of selected states that accidentally become degenerate with their parity partners [34].

Despite the considerable amount of πN data available at invariant collision energies $\sqrt{s} \geq 2$ GeV, the high-mass baryon spectrum has never been systematically explored. The known nucleon and Δ resonances with masses above 2 GeV were found already in the early single channel $\pi N \to \pi N$ partial wave analyses [35,36,37,38,39]. The results of the 1990 analysis [40] of $\pi N \to \pi N$ and $\pi N \to \pi\pi N$ data are in reasonable agreement with the previous findings [35,36,37,38,39]. The most recent GWU analysis [41,42] of πN scattering covers now energies up to $\sqrt{s}=2.6$ GeV. However, the description of the data deteriorates noticeably above $\simeq 2.4$ GeV, which is reflected in a sharp increase in the achieved χ^2. Unfortunately, the status of high-mass resonances has not yet been settled. Furthermore, the available πN data base at $\sqrt{s} \geq 1.8$ GeV is far from being complete. Specifically, for a conclusive analysis with regard to excited baryons additional polarization data are necessary. But it is rather difficult to perform the experiments in question in the near future because of the lack of suitable pion beams.

Fortunately we can use electromagnetic beams to study the excited baryons with masses above 1.8 GeV. The high-energy beams required (with $E_\gamma \geq 1.3$ GeV in the laboratory frame) are available at JLab, ELSA, GRAAL, SPring-8 and the new MAMI-C project. Data from these facilities on photo- and electro production of pseudoscalar and vector mesons should allow us to extract nucleon resonance parameters associated with excited baryon states. Among the various reaction channels with different final states, single-pion photo-production provides the most straightforward access to baryon spectroscopy. This reaction is the focus of the present work and we study it within a Regge approach.

As far as theoretical investigations are concerned πN dynamics in the so-called fourth resonance region, i.e. for energies $2 \leq \sqrt{s} \leq 3$ GeV, is practically uncharted territory. Most of the existing studies within the conventional meson-exchange picture, utilizing phenomenological Lagrangians, are restricted to energies up to the Δ (1232) excitation region, cf. [43] for a recent review. There are only very few meson-exchange models that considered πN scattering up to $\sqrt{s} \simeq 2$ GeV [44,45,46,47,48]. Also, with regard to single pion photoproduction, the majority of the investigations cover only the energy region up to $\sqrt{s} \simeq 1.5$ GeV [49,50,51,52,53]. A coupled-channel approach for the analysis of the data of photo- and electro-production of πN, ηN, and $\pi\pi N$ final states up to $\sqrt{s} \leq 2$ GeV is formulated in Ref. [54]. Finally, on a more phenomenological level, K-matrix based coupled-channel analyses of pion and photon induces reactions up to energies $\sqrt{s} \simeq 2$ GeV were presented in Refs. [55,56,57,58].

A description of the πN system within such meson-exchange models becomes very complex and difficult in practice at higher energies $\sqrt{s} \geq 2$ GeV, say. Obviously, the number of reaction channels and the number of exchange diagrams, which define the basic interactions of these models, increases tremendously and most of the pertinent parameters are not known well. In contrast, the Regge model [13,59,60,61,62,63,64], with a rel-

atively transparent parameterization of the reaction amplitude, has been fairly successful in describing hadron scattering at high energies, i.e. for photon energies above 3 GeV, say. Therefore, naturally the question arises whether the information contained in the Regge model can be exploited for investigations at lower energies and, in particular, in the transition region to those energies where the analysis of pion photoproduction data based on meson-exchange models might be still tractable. This issue is the objective of the present work.

In the present paper we utilize the Regge formalism to perform a global analysis of the world data set on charged-pion photoproduction in the high photon-energy region where resonance contributions are expected to be negligible or absent and thus the non-resonant part of the reaction amplitude can be determined reliably. In fitting the experimental results it is important to note that the Regge approach is applicable only in the small momentum transfer region. Thus, it is natural that the Regge model gradually fails to reproduce the data as the momentum-transfer increases. In our global analysis we therefore include data on differential cross sections and single and double polarization observables in the energy range $3 \leq E_\gamma \leq 8$ GeV but with the restriction $-t \leq 2$ GeV^2. The data considered were all obtained around or before 1980.

Once the parameters of the Regge model are fixed the corresponding amplitudes are extended to lower energies. Specifically, they are used to compute observables in the energy region $1.4 \leq E_\gamma \leq 3$ GeV, that corresponds roughly to invariant energies $2 \leq \sqrt{s} \leq 2.6$ GeV, and the results are confronted with data in this energy region, for example with the differential cross sections for charged pion photoproduction measured recently [65,66] in Hall A at JLab. In this energy region differences between our predictions and the data are expected. But these differences are precisely what we are after because they could be a signal for the presence of resonances and, thus, could be used to identify excited baryon states with masses $\sqrt{s} \geq 2$ GeV. Consequently, we explore at which $\sqrt{s}$ the presently available data possibly show room for additional resonance contributions and we examine the issue of which observables are the most crucial ones for excited baryon spectroscopy.

The paper is organized as follows. The formulation of the model is given in Section 2. An analysis of positive and negative pion photoproduction is given in Sections 3 and 4, respectively. In Section 5 we consider the π^-/π^+ production ratio. The paper ends with a discussion of further perspectives both in experiment and theory.

2 The Model

Because the mechanisms of charged and neutral pion photoproduction are different, we will only analyze the data for the $\gamma p \to \pi^+ n$ and $\gamma n \to \pi^- p$ reactions. Indeed for these reactions pion exchange dominates at small $-t$ whereas ω-exchange is forbidden altogether, while the situation is opposite for π^0-meson photoproduction. However, as was emphasized in Ref. [67] and will be discussed later, it is already a highly non-trivial task to obtain a Regge model fit to all of the considered world data of charged pion photoproduction.

The previous phenomenological analyses [67,68,69] of single charged pion photoproduction at high photon energies clearly indicate that a pure Regge pole model can not give an accurate description of the data. For example, it is known experimentally that the differential cross section increases when the four-momentum transfer approaches $t=0$. However, while the reaction is certainly dominated by pion exchange for small four-momentum transfer $|t|<m_\pi^2$, where m_π is the pion mass, the pion-exchange contribution alone cannot explain the data because it vanishes when $|t|$ approaches zero.

To resolve the problem it was proposed to include a "pion parity doublet" [70,71] which allows a good description of the available forward differential cross section data. But the same model could not reproduce the polarization data. Attempts have been made [67,68,72,73,74,75,76] to include absorptive corrections. Using a poor man's absorption correction [67,68] to the pion exchange enabled a good fit to the data at small $|t|$. However, a further inspection [69,77,78] indicated that the differential cross section of charged pion photoproduction increases too sharply to be explained only by the interference between the pion-exchange and Regge cut contributions.

A good description of the sharp forward peaks observed in charged pion photoproduction, while satisfying also gauge invariance, was achieved by a proper inclusion of nucleon (s or u channel) exchange. The calculations based on this approach [69] also reproduced the photon asymmetry data. Unfortunately such a gauge-invariant unitarized Regge model was not applied to perform a systematic analysis of the world data of charged pion photoproduction reactions. In this work, we will make progress in this direction.

To have a simple approach to describe the forward peaks of charged pion photoproduction differential cross sections, we do not reggeize the pion exchange. Instead, we follow previous works by assuming [69] that it contributes as a fixed pole via the electric Born term. The resulting amplitude [79,80] satisfies gauge invariance. This approach also reduces the number of parameters to be determined by a fit to the data. Such a gauge invariant amplitude for pion exchange has been employed in Refs. [69,77,81,82,83,84,85].

Before describing our model in detail let us first mention here some other problems in the previous analyses. Quite reasonable agreement between the Regge model calculations [67, 68] and data was obtained by incorporating the finite-energy sum rules (FESR) into the fitting. The use of the FESR requires reliable multipole amplitudes of pion photoproduction in the whole resonance region. Existing partial-wave analyses (PWA) [35,36,37,40] of pion-nucleon scattering have identified baryon resonances with masses up to 3 GeV. Presently the PDG listing [21] includes four baryons with a 4-star rating in the mass region from 2 to 2.5 GeV. Furthermore, the FESR applied to the $\pi^-p\rightarrow\pi^0n$ reaction distinctly illustrates [11,12,86] that the resonance region extends up to $\sqrt{s}$=3 GeV. However, the most recent GWU PWA [87] for pion photoproduction is valid only for $\sqrt{s}$ below 2.6 GeV. Therefore, an incorporation of FESR into the analysis of pion photoproduction at high energies $\sqrt{s} \geq 3$ GeV seems to be impossible at present. We thus do not include the FESR in our analysis.

Guided by the previous works described above, we here develop a gauge invariant Regge model, which combines the

Table 1. Correspondence between t-channel Regge exchanges and the helicity amplitudes F_i^- and F_i^0 ($i=1-4$). Here P is parity, J the spin, I the isospin, G the G-parity, $\mathcal{N}$ the naturalness and $\mathcal{S}$ the signature factor.

	P	J	I	G	$\mathcal{N}$	$\mathcal{S}$	Exchange
F_1^-	+1	2	1	−1	+1	+1	a_2
F_1^0	−1	1	1	+1	+1	−1	ρ
F_2^-	−1	0	1	−1	−1	+1	π
F_2^0	+1	1	1	+1	−1	−1	b_1
F_3^-	+1	2	1	−1	+1	+1	a_2
F_3^0	−1	1	1	+1	+1	−1	ρ
F_4^-	+1	1	1	−1	−1	−1	a_1
F_4^0	−1	2	1	+1	−1	+1	ρ_2

Regge pole and cut amplitudes for ρ, a_2 and b_1 exchanges as well as a gauge invariant pion-exchange Born term. Indeed at high energies the interactions before and after the basic Regge pole exchange mechanisms are essentially elastic or diffractive scattering described by Pomeron exchange. Such a scenario can be related to the distorted wave approximation and provides a well defined formulation [88,89,90,91,92] for constructing Regge cut amplitudes. This approach, which can also be derived in an eikonal formalism [93] with s-channel unitarity [73], is used in our work. Detailed discussions about the non-diffractive multiple scattering corrections involving intermediate states which differ from the initial and final states and the relevant Reggeon unitarity equations are given in Refs. [88, 94,95,96]. For simplicity we do not consider these much more involved mechanisms which would increase significantly the number of parameters to be fitted.

2.1 General structure

In our analysis we use the t-channel parity conserving helicity amplitudes F_i ($i = 1, \ldots, 4$). The F_i have proper crossing and analytic properties and definite spin-parity in the t-channel. F_1 and F_2 are the natural and unnatural spin-parity t-channel amplitudes to all orders in s, respectively. F_3 and F_4 are the natural and unnatural t-channel amplitudes to leading order in s. The amplitudes for charged pion photoproduction in the standard isospin decomposition are given by [97]:

$$F_i^{\gamma p\rightarrow\pi^+n} = \sqrt{2}[F_i^0 + F_i^-],$$
$$F_i^{\gamma n\rightarrow\pi^-p} = \sqrt{2}[F_i^0 - F_i^-]. \tag{1}$$

The correspondence between different Regge exchanges with $J\leq2$ and the amplitudes F_i^0 and F_i^- that enter into Eq. (1) is given in Table 1.

Both natural and unnatural parity particles can be exchanged in the t-channels in charged pion photoproduction provided they have isospin I=1 and G-parity G=$\pm$1. The naturalness $\mathcal{N}$ for natural ($\mathcal{N}$=+1) and unnatural ($\mathcal{N}$=−1) parity exchanges is defined as

$$\mathcal{N} = +1 \text{ if } P = (-1)^J,$$
$$\mathcal{N} = -1 \text{ if } P = (-1)^{J+1}, \tag{2}$$

where P and J are the parity and spin of the particle, respectively. Furthermore in Regge theory each exchange is denoted by a signature factor $\mathcal{S}=\pm 1$ defined as [88,60,61]

$$\mathcal{S} = P \times \mathcal{N} = (-1)^J. \tag{3}$$

2.2 Observables

The relation between the t-channel helicity amplitudes F_i and the observables can be constructed via the transformation to the s-channel helicity amplitudes S_1, S_2, N and D. Following Wiik's abbreviations [98], S_1 and S_2 are single spin flip amplitudes, N is the spin non-flip and D is the double spin flip amplitude, respectively. The asymptotic crossing relation, which is useful for the analytical evaluation of the helicity amplitudes, is given by

$$\begin{bmatrix} F_1 \\ F_2 \\ F_3 \\ F_4 \end{bmatrix} = \frac{-4\sqrt{\pi}}{\sqrt{-t}} \begin{bmatrix} 2m & \sqrt{-t} & -\sqrt{-t} & 2m \\ 0 & \sqrt{-t} & \sqrt{-t} & 0 \\ t & 2m\sqrt{-t} & -2m\sqrt{-t} & t \\ 1 & 0 & 0 & -1 \end{bmatrix} \begin{bmatrix} S_1 \\ N \\ D \\ S_2 \end{bmatrix}. \tag{4}$$

Utilizing the relations of Ref. [99] the $\gamma p \rightarrow \pi^+ n$ and $\gamma n \rightarrow \pi^- p$ observables analyzed in the present study are given by

$$\frac{d\sigma}{dt} = \frac{1}{32\pi} \left[\frac{t|F_1|^2 - |F_3|^2}{(t-4m^2)} + |F_2|^2 - t|F_4|^2 \right], \tag{5}$$

$$\frac{d\sigma}{dt}\Sigma = \frac{1}{16\pi} \left[\frac{t|F_1|^2 - |F_3|^2}{(t-4m^2)} - |F_2|^2 + t|F_4|^2 \right], \tag{6}$$

$$\frac{d\sigma}{dt}T = \frac{\sqrt{-t}}{16\pi} \operatorname{Im} \left[\frac{-F_1 F_3^*}{(t-4m^2)} + F_4 F_2^* \right], \tag{7}$$

$$\frac{d\sigma}{dt}R = \frac{\sqrt{-t}}{16\pi} \operatorname{Im} \left[\frac{-F_1 F_3^*}{(t-4m^2)} - F_4 F_2^* \right], \tag{8}$$

where the appropriate isospin combinations of the F_i's according to Eq. (1) need to be taken. The relations in Eqs. (5) - (8) allow one to obtain constraints for the t-channel helicity amplitude directly from experimental observables. Note that Eq. (4) is appropriate only at $s \gg t$, since it does not account for the higher order corrections that are proportional to $t/4m^2$. The amplitudes F_i are related to the usual CGLN invariant amplitudes A_i [97] by

$$\begin{aligned} F_1 &= -A_1 + 2mA_4, \\ F_2 &= A_1 + tA_2, \\ F_3 &= 2mA_1 - tA_4, \\ F_4 &= A_3. \end{aligned} \tag{9}$$

Expressions for the experimental observables in terms of the amplitudes A_i are listed, for instance, in Ref. [100]. The often used multipole amplitudes can be constructed from the helicity amplitudes using the relations given in Ref. [101].

2.3 Structure of the amplitudes

The pion photoproduction amplitude of our model is given by

$$F_i = F_i^{(\pi)} + F_i^{(Regge)}, \tag{10}$$

where contributions from Regge exchanges of the ρ, a_2 and b_1 trajectories are taken into account. Their concrete structure and parameterization is described in detail in the next subsection. As mentioned, the contribution from pion exchange is treated differently and will be discussed and described in detail in a separate subsection below.

2.3.1 Regge amplitudes

Similar to the particle-exchange Feynman diagram, each reaction amplitude F is factorized in terms of a propagator G and a vertex function β

$$F_i^{(Regge)}(s,t) \sim \beta_i \times G. \tag{11}$$

However, there is a difference in defining the propagator. The basic reaction mechanism in the Regge model is not associated with the exchange of certain particles but with the exchange of certain quantum numbers. Therefore, the mass of the exchanged particle does not appear in the amplitudes explicitly. Accordingly, the usual Feynman propagator, which contains the mass m of the exchange particle, is replaced by the Regge propagator

$$G \sim \frac{1}{t-m^2} \Rightarrow \frac{1+\mathcal{S}\exp[-i\pi\alpha(t)]}{\sin[\pi\alpha(t)]\ \Gamma[\alpha(t)+1]} \left[\frac{s}{s_0} \right]^{\alpha(t)-1}, \tag{12}$$

where s_0=1 GeV^2 is a parameter for defining a dimensionless amplitude, $\mathcal{S}$ is the signature factor given in Table 1 and $\alpha(t)$ is the Regge trajectory. The trajectories are the most essential part of the Regge model and they are defined by the spins (J) and masses (m_J) of the particles with a fixed G-parity, $\mathcal{N}$ and $\mathcal{S}$. Specifically, the function $\alpha(t)$ characterizing the trajectory is obtained from the relation $\alpha(m_J) = J$ applied to those particles that form the trajectory. The trajectories pertinent to our approach will be discussed below.

Obviously the Regge propagator of Eq. (12) accounts for the whole family of particles or poles, which lie on a certain trajectory, where the trajectory is *named after* the lowest J state. Thus, by considering different trajectories constructed in the unphysical $t \geq 0$ region one can effectively include all possible exchanges allowed by the conservation of quantum numbers. This is an obvious advantage of the Regge theory, since with increasing energy it is necessary to include the exchanges of higher-mass and higher-spin particles and a description within standard relativistic meson-exchange models would become too involved or even unmanageable.

From Eq. (12), we see that the factor $\sin[\pi\alpha(t)]$ would generate also poles at $t \leq 0$ when $\alpha(t)$ assumes the values $0, -1, \ldots$. The function $\Gamma[\alpha(t)+1]$ is *introduced* to suppress those poles that lie in the scattering region because

$$\frac{1}{\Gamma[\alpha(t)+1]} = -\frac{\sin[\pi\alpha(t)]}{\pi}\Gamma(\alpha(t)). \tag{13}$$

However, the suppression of the poles in the physical region can be done by other means too. This issue will be discussed below when we introduce the concrete parameterization of the Regge amplitudes that we use.

The structure of the vertex function β of Eq. (11) is defined by the quantum numbers of the particles at the interaction vertex, similar to the usual particle exchange Feyman diagram. This vertex function is taken to be real and hence ρ, the ratio of the real to imaginary parts of the reaction amplitude, is given by

$$\rho = \frac{\mathrm{Re}\,F}{\mathrm{Im}\,F} \propto -\frac{\mathcal{S} + \cos[\pi\alpha(t)]}{\sin[\pi\alpha(t)]}, \tag{14}$$

for a specific Regge exchange, i.e. simply by the phase of Eq. (12). This phase is required by the fixed-t dispersion relation and is well verified experimentally[2].

The Regge amplitudes used in our model calculation are of the form

$$F_i^{(Regge)}(s,t) = \sum_j [F_{ij}^{(pole)}(s,t) + F_{ij}^{(cut)}(s,t)], \tag{15}$$

where $j = 1, 2, 3$ denote the trajectories a_2, ρ and b_1, respectively. (Note that we do not consider the amplitude F_4 and the corresponding trajectories a_1 and ρ_2 in the present investigation for reasons that are discussed later.) Each of the pole amplitudes are parameterized as [88] (suppressing the subscripts ij)

$$F^{(pole)}(s,t) = \beta(t)\frac{1 + \mathcal{S}\exp[-i\pi\alpha(t)]}{\sin[\pi\alpha(t)]}\left[\frac{s}{s_0}\right]^{\alpha(t)-1}, \tag{16}$$

where $\beta(t)$ is the residue function which accounts for the t-dependence and the coupling constant at the interaction vertex, and $\mathcal{S}$ is the signature factor given by Eq. (3) and listed in Table 1.

The residue functions $\beta(t)$ used in our analysis are compiled in Table 2. They are similar to the ones used in some of the previous analyses [67,69]. The factor $\alpha(t)[\alpha(t)+1]$ in Table 2 is used to suppress the poles of the propagator in the scattering region. Alternatively this suppression can be achieved [88] by introducing the $\Gamma[\alpha(t)]$ function as seen in Eqs. (12) and (13). One can also introduce a factor $[\alpha(t)+n]$ with $n=2,3,\ldots$ to suppress poles at large $-t$. However, we do not apply the Regge model beyond $|t|=2$ GeV, and therefore such a suppression factor is not considered. We should mention that in some studies [102] it was proposed to drop the $\alpha(t)$ factor for the ρ pole exchange. But we keep this factor in our model. In fact, we found that it has practically no influence on the achieved χ^2 of the fit.

The trajectories are of the following linear form:

$$\alpha(t) = \alpha_0 + \alpha' t, \tag{17}$$

where the parameters (α_0, α') for the considered a_2, ρ and b_1 trajectories are taken over from analyses of other reactions [88, 103]. Explicitly we have for the considered a_2, ρ and b_1 trajectories

$$\begin{aligned} \alpha_{a_2} &= \alpha_1 = 0.4\ + 0.99\,t \\ \alpha_\rho &= \alpha_2 = 0.53 + 0.8\,t \\ \alpha_{b_1} &= \alpha_3 = 0.51 + 0.8\,t\,. \end{aligned} \tag{18}$$

---

[2] For instance, the ratio ρ can be measured directly in forward elastic scattering.

Table 2. Parameterization of the $\beta(t)$ functions for the amplitudes F_i, ($i=1-3$). Here c_{ij} is the coupling constant where the double index refers to the amplitude and the type of exchange, as specified in the Table, while $\alpha_j(t)$ denotes the trajectory for the type of exchange. These trajectories are given by Eqs. (18) and (20).

	Residue function $\beta(t)$	Exchange	j
	Pole amplitudes		
F_1	$c_{11}\,\alpha_1(t)\,[\alpha_1(t)+1]$	a_2	1
F_1	$c_{12}\,\alpha_2(t)\,[\alpha_2(t)+1]$	ρ	2
F_2	$c_{23}\,t\,\alpha_3(t)\,[\alpha_3(t)+1]$	b_1	3
F_3	$c_{31}\,t\,\alpha_1(t)\,[\alpha_1(t)+1]$	a_2	1
F_3	$c_{32}\,t\,\alpha_2(t)\,[\alpha_2(t)+1]$	ρ	2
	Cut amplitudes		
F_1	$c_{14}\,[\alpha_4(t)+1]\,\exp[d_4 t]$	a_2	4
F_1	$c_{15}\,\alpha_5(t)\,\exp[d_5 t]$	ρ	5
F_1	$c_{16}\,[\alpha_6(t)+1]\,\exp[d_6 t]$	b_1	6
F_2	$c_{24}\,[\alpha_4(t)+1]\,\exp[d_4 t]$	a_2	4
F_2	$c_{25}\,\alpha_5(t)\,\exp[d_5 t]$	ρ	5
F_2	$c_{26}\,[\alpha_7(t)+1]\,\exp[d_6 t]$	b_1	6
F_3	$c_{34}\,[\alpha_4(t)+1]\,\exp[d_4 t]$	a_2	4
F_3	$c_{35}\,\alpha_5(t)\,\exp[d_5 t]$	ρ	5
F_3	$c_{36}\,[\alpha_6(t)+1]\,\exp[d_6 t]$	b_1	6

In defining the Regge cut amplitudes $F^{(cut)}$ of Eq. (15) we use the following parameterization based on the absorption model [60,104,105,106,69] (suppressing again the subscripts)

$$F^{(cut)}(s,t) = \frac{\beta(t)}{\log{(s/s_0)}}\frac{1 + \mathcal{S}\exp[-i\pi\alpha_c(t)]}{\sin[\pi\alpha_c(t)]}\left[\frac{s}{s_0}\right]^{\alpha_c(t)-1}, \tag{19}$$

with the trajectories defined by

$$\alpha_c = \alpha_0 + \frac{\alpha'\alpha'_P\,t}{\alpha' + \alpha'_P}, \tag{20}$$

where α_0 and α' were taken from the pole trajectory given by Eqs. (17) and (18), and $\alpha'_P=0.2$ GeV^{-2} is the slope of the pomeron trajectory. The residue functions $\beta(t)$ of Eq. (19) are also listed in Table 2, where the relevant cut trajectories are numerated as α_4, α_5, α_6 for the a_2, ρ and b_1 cut amplitudes, respectively.

2.3.2 Pion-exchange amplitude

As already mentioned in the beginning of this section, we do not reggeize the pion exchange. Instead, we follow previous works by assuming [69] that it contributes as a fixed pole via the electric Born term. Indeed, pion exchange dominates the region $-t < m_\pi^2$ and in this region the Regge propagator can be savely replaced by the Feyman propagator. The resulting amplitude [79,80] satisfies gauge invariance in photoproduction. This approach allows us to describe the forward peaks of charged pion photoproduction differential cross sections in

a simple way. It also reduces the number of parameters to be fitted by the data.

The gauge invariant pion Born term $F_i^{(\pi)}(s,t)$ is calculated [69,81,82,83,97,107] from the usual pion and nucleon exchange Feynman diagrams for $\gamma N \to \pi N$, but keeping only the pure electric coupling in the γNN vertex. Explicitly, the invariant amplitudes for the $\gamma p \to \pi^+ n$ reaction are given by

$$A_1 = -\frac{eg}{s - m_N^2} f(t) ,$$
$$A_2 = \frac{2eg}{(s - m_N^2)(t - m_\pi^2)} f(t) . \tag{21}$$

(The relation between the invariant and the helicity amplitudes is given by Eq. (9).) Here m_N and m_π stand for the nucleon and pion mass, respectively, and e and g are the electric and πNN coupling constants taken as $e^2/4\pi = 1/137$ and $g^2/4\pi = 13.76$. Following the standard procedure [69] a phenomenologicl form factor $f(t)$ is included,

$$f(t) = a \exp(bt), \tag{22}$$

where a and b are free parameters to be determined by a fit to the data. For the $\gamma n \to \pi^- p$ reaction the gauge invariance of the pion exchange can be restored by the u-channel nucleon exchange [108] with invariant amplitudes taken as

$$A_1 = \frac{eg}{u - m_N^2} f(t) ,$$
$$A_2 = -\frac{2eg}{(u - m_N^2)(t - m_\pi^2)} f(t) . \tag{23}$$

Indeed for small $-t \leq m_\pi^2$ where the pion exchange dominates, the propagators for s and u channels fulfill approximately

$$-u + m_N^2 \simeq s - m_N^2, \tag{24}$$

when neglecting terms smaller than the pion mass squared. That is why in Refs. [69,81] the u-channel correction to the gauge invariance was not specified explicitly and only s channel invariant amplitudes were given.

As is obvious from Eqs. (21) and (23) in conjunction with Eq. (9), the pion-exchange contribution derived above contributes to the helicity amplitudes F_1 to F_3 while the reggeized pion exchange would contribute only to F_2, cf. Table 1.

2.4 Parameters of the model

With the formulation presented above the considered reaction amplitude has 19 free parameters. As discussed in section 1, we fix these parameters by a fit to the (π^+ and π^-) production data at energies $3 \leq E_\gamma \leq 8$ GeV and momentum-transfers $-t \leq 2$ GeV^2. Some general information on those data [109] is given in the following sections where the results are discussed.

In order to avoid any dependence of the fit on the starting parameters we used the random walk method to construct the initial set of parameters and we repeated the minimization procedure many times. Furthermore, an additional examination was done by exploring the results for the parameter correlation-matrix in order to inspect the stability of the found minimum.

Table 3. Parameters of the model. Here c_{ij} is the coupling constant for the ith amplitude and the type of exchange, d_j is a cut-off parameter for the Regge cut amplitude, while a and b are the parameters of the Born term form factor, cf. Table 2 and Eq. (22).

j	c_{ij}			d_j
	$i=1$	$i=2$	$i=3$	
1	-30.1	-	103.8	-
2	36.1	-	31.0	-
3	-	-8.4	-	-
4	164.0	-42.0	348.6	1.46
5	-286.8	127.1	-22.1	0.75
6	271.9	-141.3	5.9	0.78
	$a = 0.8$		$b = 1.56$	

The data for both the positive and negative pion photoproduction are fitted simultaneously. The resulting parameters of the model are given in Table 3. The achieved χ^2/ndf amounts to 1.4. We find that some of the data from different experiments are slightly inconsistent. There is no way to improve the confidence level of our global analysis unless these inconsistent data are removed from the data base. However, it is difficult to find meaningful criteria for pruning the data base.

2.5 Experimental constraints on F_4

As seen in Table 2, we do not include the amplitude F_4 in our analysis. The F_4 amplitude is given by the $J^{PC}=1^{++}$ and $J^{PC}=2^{--}$ exchanges and their cuts. Those contributions correspond to the exchanges of the a_1, f_1, ρ_2 and ω_2 mesons with the indicated quantum numbers[3], where the latter two are not well established experimentally [21]. In addition, the relevant amplitudes are small because the corresponding trajectories are low-lying in the J-plane [110]. That were the reasons why the F_4 amplitude was neglected in many previous studies of charged-pion photoproduction.

By inspecting the relation between the amplitudes F_i and the observables one can immediately conclude that the single polarization data on target (T) and recoil (R) asymmetries[4] are very crucial to determine the role of F_4. Indeed if $T=R$ exactly then it follows that $F_4=0$. A direct measurement of the $R-T$ difference allows access to F_4 in a model independent way because

$$R - T = 4\pi \sqrt{-t} \, \text{Im}[\, F_4 F_2^* \,] , \tag{25}$$

and because the F_2 amplitude is well established from the investigation of various reactions [99] dominated by π-meson exchange. Furthermore, without any model assumption, the following Worden inequalities [92] can be derived from the rela-

---

[3] Formerly the a_1 and ρ_2 mesons were called A_1 and Z, respectively [88]

[4] Note that in some publications of experimental results the notation is different. Specifically, for the recoil asymmetry P is used (instead of R) and for the polarized photon asymmetry A (instead of Σ).

Table 4. The $\gamma p \to \pi^+ n$ data on differential cross section analyzed in the present paper.

E_γ (GeV)	$\sqrt{s}$ (GeV)	$-t_{min}$ (GeV^2)	$-t_{max}$ (GeV^2)	Reference
Differential cross section, $d\sigma/dt$

E_γ (GeV)	$\sqrt{s}$ (GeV)	$-t_{min}$ (GeV^2)	$-t_{max}$ (GeV^2)	Reference
1.1	1.72	0.47	0.71	[65]
1.1	1.72	4.1×10^{-3}	0.41	[112]
1.48	1.91	0.024	0.24	[113,114]
1.62	1.98	1.1×10^{-3}	0.34	[113,114]
1.65	1.99	0.42	1.18	[65]
1.77	2.05	1.3×10^{-3}	0.38	[113,114]
1.8	1.99	0.47	1.32	[65]
1.99	2.15	1.5×10^{-3}	0.44	[113,114]
2.18	2.23	1.6×10^{-3}	0.6	[113,114]
2.38	2.31	1.8×10^{-3}	0.66	[113,114]
2.48	2.35	0.69	1.95	[65]
2.51	2.36	0.126	0.323	[115]
2.63	2.41	2×10^{-3}	0.74	[113,114]
3.25	2.64	0.124	0.45	[115]
3.32	2.67	0.96	3.64	[65]
3.4	2.69	3×10^{-3}	0.4	[116]
3.4	2.69	0.09	0.33	[117]
3.41	2.7	0.374	1.396	[118]
3.4-4.0	2.69-2.9	0.25	1.31	[119]
4.0	2.9	0.95	5.14	[120]
4.15	2.94	2.28	4.1	[65]
4.17	2.95	0.09	0.551	[115]
4.4	3.02	6.77	7.08	[121]
5.0	3.2	0.01	0.61	[116]
5.0	3.2	0.19	1.45	[117]
5.0	3.2	1.44	6.8	[120]
5.0	3.2	2×10^{-4}	1.15	[122]
5.53	3.36	4.75	5.6	[65]
7.5	3.87	1.95	11.63	[120]
8.0	3.99	5.1×10^{-4}	2.13	[122]
11.0	4.64	8×10^{-4}	2.06	[122]
16.0	5.56	1.2×10^{-3}	1.95	[122]

Table 5. The $\gamma p \to \pi^+ n$ data on the polarized photon asymmetry Σ (denoted formerly as A [92]), target asymmetry T, and the recoil symmetry R (denoted formerly as P [92]) analyzed in the present paper.

E_γ (GeV)	$\sqrt{s}$ (GeV)	$-t_{min}$ (GeV^2)	$-t_{max}$ (GeV^2)	Reference
Polarized photon asymmetry Σ
1.55	1.95	0.15	1.39	[132]
1.65	1.99	0.16	1.5	[132]
1.95	2.13	0.2	2.08	[132]
2.25	2.26	0.23	1.89	[132]
2.5	2.36	0.02	0.31	[123]
3.0	2.55	0.15	1.16	[124]
3.4	2.69	0.01	0.6	[123]
3.4	2.69	2.6×10^{-3}	0.01	[133]
5.0	3.2	0.1	0.4	[123]
16.0	5.56	5.5×10^{-3}	1.5	[125]
Target asymmetry T
1.55	1.95	0.15	1.39	[132]
1.65	1.99	0.16	1.5	[132]
1.95	2.13	0.2	2.08	[132]
2.25	2.26	0.23	1.89	[132]
2.5	2.36	0.1	0.87	[130]
3.4	2.69	0.1	1.14	[130]
5.0	3.2	0.1	1.25	[130]
5.0	3.2	0.019	1.02	[131]
16.0	5.56	0.019	0.62	[131]
Recoil asymmetry R
1.55	1.95	0.15	1.39	[132]
1.65	1.99	0.16	1.5	[132]
1.95	2.13	0.2	2.08	[132]
2.25	2.26	0.23	1.89	[132]

tion between the F_i amplitudes and the observables:

$$|R - T| \leq 1 - \Sigma\,, \qquad (26)$$
$$|R + T| \leq 1 + \Sigma\,, \qquad (27)$$
$$|D| \leq \sqrt{1 - \Sigma^2}\,, \qquad (28)$$

where D denotes the double polarization parameters G, H, E and F, which are given in Refs. [99,111]. In addition, the observables obey the following equations [99,92]

$$E^2 + F^2 + G^2 + H^2 = 1 + R^2 - \Sigma^2 - T^2\,, \qquad (29)$$
$$FG - EH = R - T\Sigma\,, \qquad (30)$$

which allow to construct F_4 from the full set of single and double polarization measurements.

Unfortunately, there are no data for both T and R asymmetries available for the charged-pion photoproduction at photon energies explored in the present study. The data [123,124,125] at $3\leq E_\gamma\leq16$ GeV indicate for the photon polarized asymmetry

$\Sigma\simeq0.8$. Following Eq. (26) this implies that $|R-T|\leq0.2$, suggesting that the F_4 amplitude could be not negligible. The data available for T and R at $E_\gamma\leq2.25$ GeV imply that, within the experimental uncertainties, $T\simeq R$. At higher energies, $E_\gamma\geq2$ GeV, experimental results for T and R [126,127,128,129] are available only for neutral pion photoproduction. Those suggest also that $T\simeq R$. However, the statistical uncertainty of these data is large and at $E_\gamma\leq4$ GeV the comparison of target and recoil asymmetries requires an interpolation in t and an extrapolation in the photon energy.

Certainly, apart from the mentioned experimental indications, there are no fundamental reasons to ignore the F_4 contribution. Indeed, we did attempt to include the F_4 amplitude in the global fit following the trajectory parameters given in Ref. [88]. However, it turned out that the fit is insensitive to that contribution. In addition, the most crucial data available [130, 131] at $E_\gamma>3$ GeV for target asymmetries are afflicted with large errors. Thus, finally we decided to neglect F_4 in the present study.
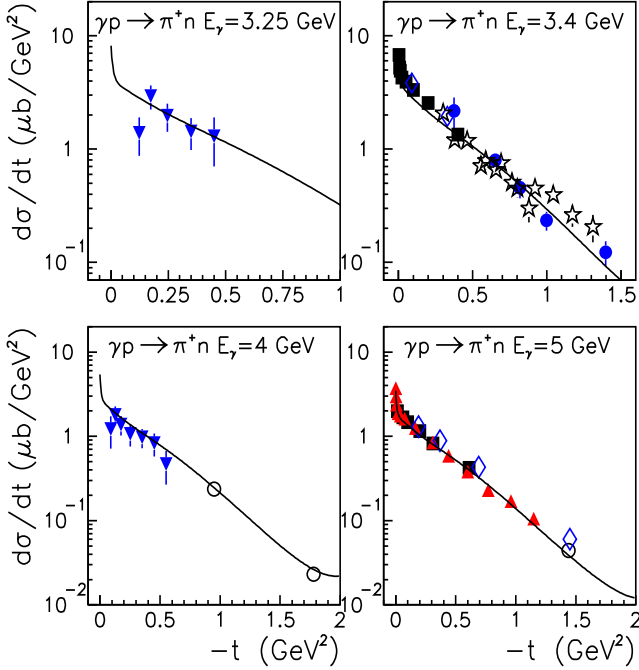
Fig. 1. The $\gamma p \to \pi^+ n$ differential cross section as a function of $-t$, the four-momentum transfer squared, at different photon energies E_γ. The data are taken from Refs. [116] (filled squares), [117] (open diamonds), [122] (filled triangles), [115] (inverse filled triangles), [118] (filled circles), [119] (open stars), and [120,121] (open circles). The solid lines show results of our model calculation based on the parameters listed in Table 3.

3 Results for $\gamma p \to \pi^+ n$

This section is organized as follows. First we compare the results based on our model with the data included in our global fit, i.e. data in the region $3 \leq E_\gamma \leq 8$ GeV and $-t \leq 2$ GeV^2. Some general information on those data is listed in Tables 4 and 5. We also confront our model with the available data at the higher energies E_γ=11 and 16 GeV which were not included in our fit. Information on those data are listed too in the Tables.

Then we look at data for $1.4 < E_\gamma < 3$ GeV where our Regge-model results can be considered as predictions. The lowest photon energy is chosen in order to cover invariant masses down to $\sqrt{s} \simeq 2$ GeV, which is roughly the lower end of the fourth resonance region. Note that at these energies we definitely expect to be in disagreement with the data. But we regard such a disagreement as the starting point for exploring possible contributions from nucleon resonances. Thus our interest in that energy range is to examine systematically for which observables and in which kinematical regions discrepancies between our predictions and available data occur.

Finally, we compare our predictions with the most recent data [65,66] for differential cross sections at $1.1 \leq E_\gamma \leq 5.5$ GeV, collected by the Hall A Collaboration at JLab. The main interesting feature of these data is that they cover a region of fairly large momentum transfer $-5.6 \leq t \leq -0.4$ GeV^2 and thus provide a window for examining the transition from non-perturbative QCD to perturbative QCD. Also here we are guided by the aim to learn how the amplitudes generated from our Regge model
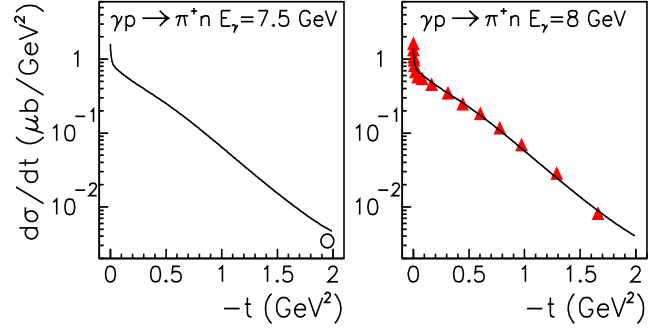

Fig. 2. The $\gamma p \to \pi^+ n$ differential cross section as a function of $-t$ at different photon energies E_γ. The data are taken from Refs. [122] (filled triangles) and [120,121] (open circle). The solid lines show results of our model calculation.

could be used to investigate the reaction mechanisms relevant in this rather complex and exciting transition region. However, the solution of this problem is beyond the scope of this paper and will be postponed to future investigations.

3.1 Results at $E_\gamma \geq 3$ GeV

Our results for the $\gamma p \to \pi^+ n$ differential cross sections are presented in Figs. 1 and 2. The model reproduces the data quite well. Note that the differential cross sections increase sharply when approaching t=0 and can only be fitted by using the gauge invariant pion exchange term $F^{(\pi)}$ as described in subsection 2.3.2. It will be interesting to see whether this particu-
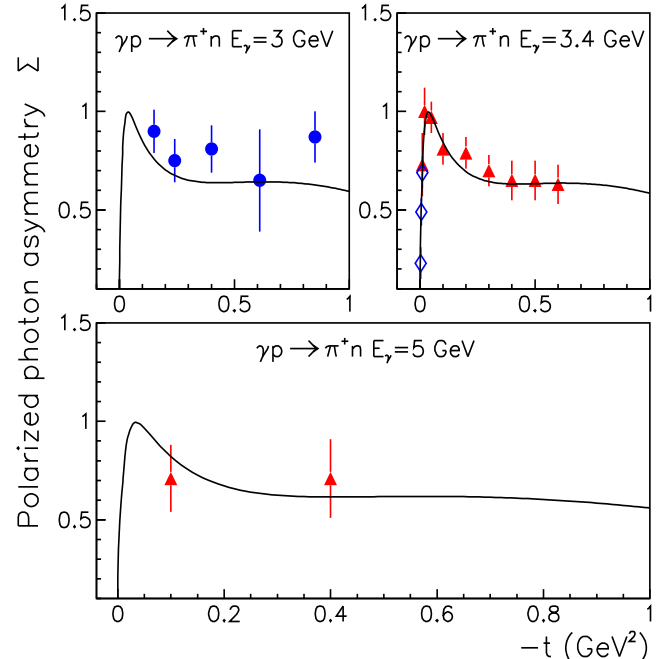

Fig. 3. Polarized photon asymmetry for the reaction $\gamma p \to \pi^+ n$ as a function of $-t$ at different photon energies E_γ. The data are taken from Refs. [123] (filled triangles), [124] (filled circles) and [133] (open diamonds). The solid lines are the results of our calculation.
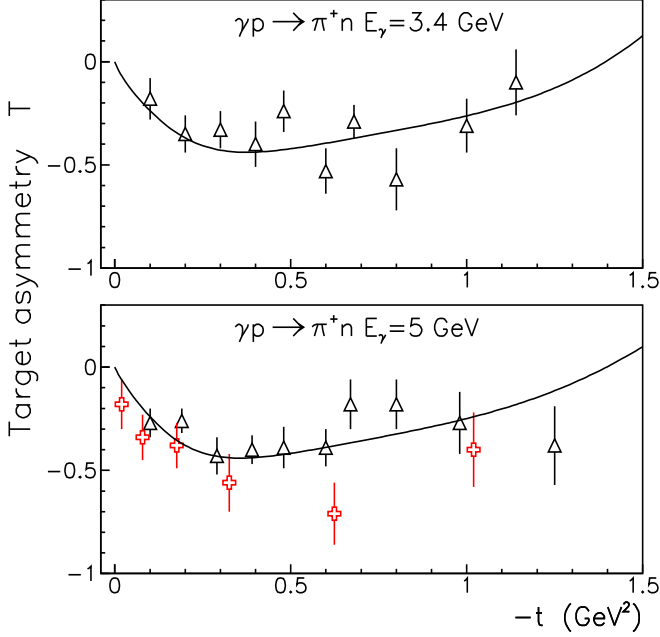
Fig. 4. Target asymmetry T for the reaction $\gamma p \rightarrow \pi^+ n$ as a function of $-t$ at different photon energies E_γ. The data are taken from Refs. [130] (open triangles) and [131] (open crosses). The solid lines show results of our model calculation.

Fig. 5. The $\gamma p \rightarrow \pi^+ n$ differential cross section (upper panel) and polarized photon, Σ and target T asymmetries as a function of $-t$ at the photon energies E_γ=11 GeV and 16 GeV. The data are taken from Refs. [122] (filled triangles), [125] (asterisk) and [131] (open crosses). The solid lines show results of our model calculation.

lar feature can give us some clue about how the Regge model can be connected with meson-exchange models. In the latter a gauge invariant pion-exchange, derived from phenomenological Lagrangians, is also a crucial ingredient in describing the charged pion photoproduction at lower energies $\sqrt{s} \leq 2$ GeV. In particular, it will be instructive to compare the multipole amplitudes in the transition region $\sqrt{s} \simeq 2-3$ GeV where both models could be equally successful in describing the non-resonant contribution around t=0. Our investigation on this issue will be reported elsewhere.

Fig. 3 presents results of our fits to the data for the photon asymmetry Σ. The photon asymmetry Σ is defined by

$$\Sigma = \frac{d\sigma_\perp - d\sigma_\parallel}{d\sigma_\perp + d\sigma_\parallel} , \qquad (31)$$

where $d\sigma_\perp$ ($d\sigma_\parallel$) is the cross section from measurements with photons polarized in the direction perpendicular (parallel) to the γ-π scattering plane.

Within the Regge model the data on Σ can be used [134, 135, 136] to separate the contributions from natural and unnatural parity exchanges. According to Ref. [134] the differential cross section $d\sigma_\perp$ ($d\sigma_\parallel$) is due to unnatural (natural) parity exchanges. Thus, a large and positive Σ at forward angles, seen in the left panel of Fig. 3, indicates the dominance of unnatural parity exchanges and can be described by the pion-exchange mechanism [124, 133]. The data show that Σ is positive and almost constant, suggesting that $d\sigma_\perp > d\sigma_\parallel$ over the whole considered range of t. Hence, the photoproduction of π^+ photoproduction is indeed dominated by unnatural parity exchanges in the kinematic region considered.
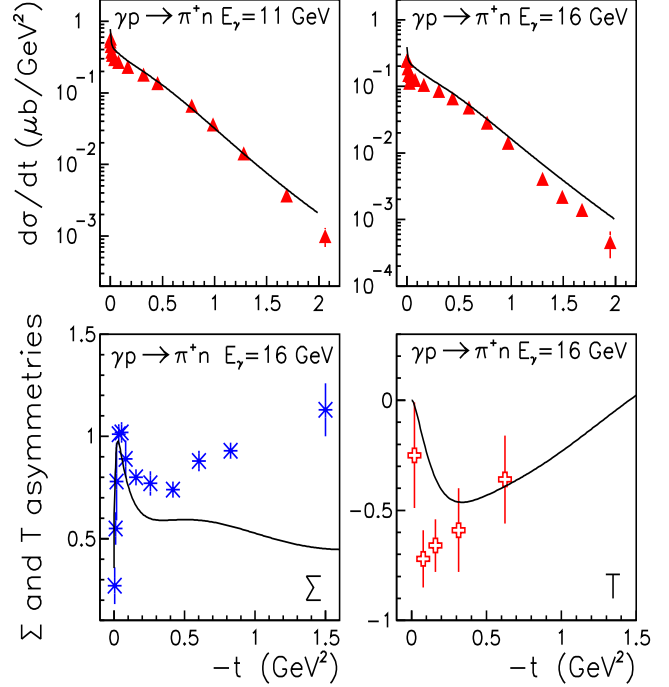
Our fit to the data on the target asymmetry T is shown in Fig. 4. The data were obtained [130, 131] using a buthanol frozen spin target. Within the experimental uncertainties the data are well reproduced by our calculation. To test the constructed model, we first compare our predictions with the data available at higher energies, namely at E_γ=11 GeV and 16 GeV. Note that these data were not included in our global fits. The upper panel of Fig. 5 shows the differential cross section for $\gamma p \rightarrow \pi^+ n$, which is well reproduced by the model calculation. The lower panel of Fig. 5 displays results for the polarized photon asymmetry Σ and the target asymmetry T for E_γ=16 GeV. Here deficiencies of the model are apparent.

To remove the remaining discrepancies, specifically in the polarization observables, one may have to include the F_4 contribution which has been neglected in the present fit, as discussed in subsection 2.5. Indeed, the F_4 contribution is primarily sensitive to the difference between the recoil (R) and target (T) asymmetries, as given by Eq. (25). Unfortunately, there is no experimental information available for R. Apparently more data on Σ, T and R as well as other polarization observables are needed for making further progress.

3.2 Predictions at lower energies

As was stressed in many studies [88, 92, 106], the Regge theory is phenomenological in nature. There is no solid theoretical derivation that allows us to establish explicitly the ranges of t and s where this formalism is applicable. Nevertheless,
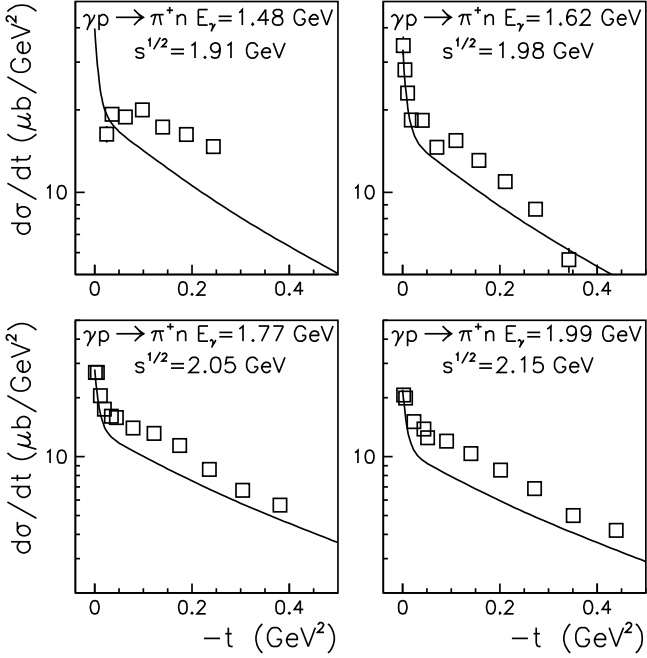
Fig. 6. The $\gamma p \rightarrow \pi^+ n$ differential cross section as a function of $-t$ at different photon energies E_γ. Here $\sqrt{s}$ is the γp invariant collision energy. The data are taken from Refs. [113,114] (open squares). The solid lines show results of our model calculation.

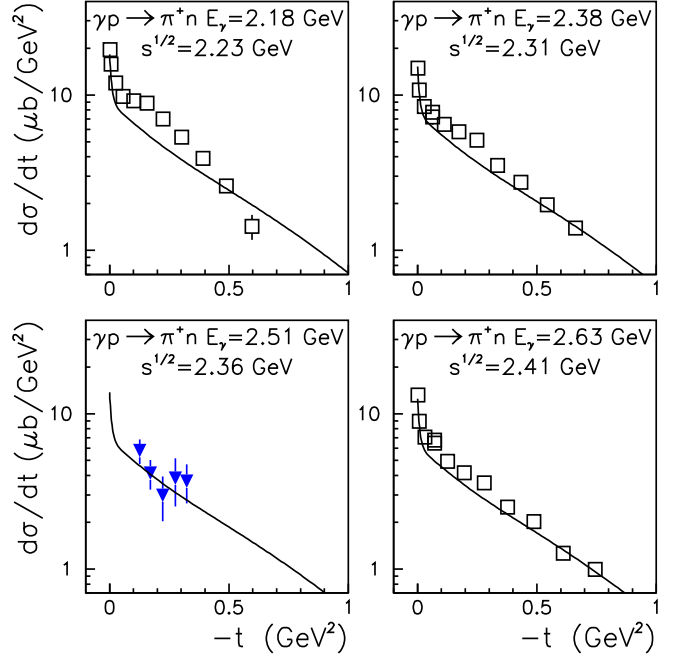**Fig. 7.** The $\gamma p \rightarrow \pi^+ n$ differential cross section as a function of $-t$ at different photon energies E_γ. The data are taken from Refs. [115] (inverse close triangles) and [113,114] (open squares). The solid lines show results of our model calculation.

following the usual arguments based on the analytic properties of the scattering amplitudes in the complex angular momentum plane, it is reasonable to assume that the Regge model constructed above is valid for describing quantitatively the exchange mechanisms down to energies of around $E_\gamma \simeq 3$ GeV which corresponds to $\sqrt{s} \simeq 2.55$ GeV. Since there are several well-identified nucleon resonances [21] in the energy range up to the range of $\sqrt{s} \simeq 2.6$ GeV, identified in partial wave analyses [35,36,37,38,40,56,137,138] of pion-nucleon scattering, we expect that deviations of our predictions from the data will start to show up for energies from $E_\gamma \simeq 3$ GeV downwards and it is obvious that those discrepancies could be a signal for possible contributions from nucleon resonances. Thus, our specific interest here is to examine carefully this transition energy region and to single out those observables which can be used most effectively to establish the presence of resonances or even to extract nucleon resonance parameters.

The solid lines in Figs. 6,7 show our predictions for the $\gamma p \rightarrow \pi^+ n$ differential cross sections at $1.48 \leq E_\gamma \leq 2.63$ GeV in comparison with the data. Here we also indicate the corresponding γp invariant mass $\sqrt{s}$. We see from Fig. 7 that our predictions are in reasonable agreement with the experimental results [115,113,114] down to $E_\gamma = 2.38$ GeV, which corresponds to an invariant mass of $\sqrt{s} \simeq 2.31$ GeV. At those energies there is not much room for additional contributions within the t range covered by the experiments. As seen from Figs. 6 and 7, our predictions start to deviate more systematically from the data below $E_\gamma = 2.18$ GeV or $\sqrt{s} = 2.23$ GeV.

Our predictions for the photon asymmetry Σ are presented in Fig. 8. Here we see very large differences between our predictions (solid lines) and the data for photon energies $E_\gamma \leq$

2.25 GeV. On the other hand, the model is in good agreement with data on Σ at the photon energy E_γ=2.5 GeV, which corresponds to $\sqrt{s}$=2.36 GeV. But here one should keep in mind that the data cover only a very small range of t. Since the polarized photon asymmetry varies substantially as a function of the four-momentum transfer squared within the considered range $1.95 \leq \sqrt{s} < 2.36$ GeV, one might consider this as an indication for the excitation of baryonic resonances.

Fig. 9 presents data on the target polarization T (filled circles and triangles) and the recoil polarization R (open circles) together with the model results. Please recall that in our model we assume F_4=0 and, hence, the predictions for these two observables are the same, cf. Eqs. (7) and (8). Thus, there is only one (solid) line in each panel of Fig. 9. There are some deviations of our model result from the data at photon energies below 2.25 GeV. However, the accuracy of the data is not sufficient to draw further and more concrete conclusions. Indeed, it looks as if both R and T oscillate around the value zero. It is interesting to note that the data in Fig. 9 suggest that $T \simeq R$ within the experimental uncertainties. Thus, our assumption that $F_4 = 0$ is in line with the experimental evidence. Nevertheless, more precise data on these two observables would be rather useful for drawing more definite conclusions on F_4.

3.3 Comparison with the JLab data

The most recent data on charged meson photoproduction were obtained by the Hall A Collaboration [65,66] at JLab. These data cover a wide range of photon energies ($1.1 \leq E_\gamma \leq 5.53$
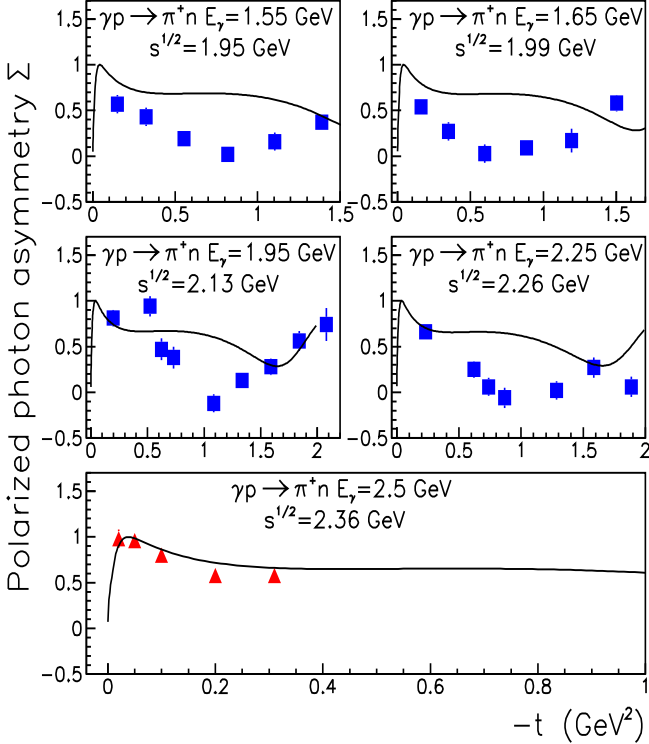
Fig. 8. Polarized photon asymmetry from $\gamma p \to \pi^+ n$ reaction as a function of $-t$ at different photon energies. The data are taken from Refs. [132] (squares) and [123] (filled triangles). The solid lines show results of our model calculation.

Fig. 9. Target (T) (filled circles and triangles), and recoil asymmetry (R) (open circles) for $\gamma p \to \pi^+ n$ as a function of $-t$ at different photon energies E_γ. The data are taken from Refs. [132] (filled and open circles) and [130] (triangles). The solid lines are our result.

GeV) and squared four-momentum transfers ($0.4 \leq -t \leq 5.6$ GeV^2).

We first consider the data at low energies, $E_\gamma \leq 2.48$ GeV. Fig. 10 presents differential cross sections as a function of the squared four-momentum transfer collected from different experiments [115, 113, 114, 112, 65]. Here the JLab data [65] correspond to the stars and they are consistent with previous measurements. (Note that the other data were taken, in general, at slightly different energies, cf. Figs. 1, 2, 6, 7.) The solid lines are the results of our model calculation. They are in line with the JLab data points for $E_\gamma \geq 1.65$ GeV and for small $-t$, but deviate from the data at -t around or above 1 GeV. The large discrepancy at $E_\gamma = 1.1$ GeV or $\sqrt{s} = 1.7$ GeV is to be expected because in this energy region there should be additional contributions from well established resonances.

In Fig. 11 we compare our predictions at $E_\gamma \geq 3.0$ GeV with the JLab data (stars) and with all other available data. Note that the older data shown by open circles in the figure for $E_\gamma = 4.1$ GeV and 5.53 GeV are actually from measurements at $E_\gamma = 4.0$ GeV and 5.0 GeV, respectively. However, these small energy differences are not important for our discussions here. Obviously only two of the JLab data points at the photon energy $E_\gamma = 3.3$ GeV are in the $-t \leq 2$ GeV^2 region. These are well described by our model prediction. Furthermore, they are also in good agreement with data from earlier measurements [116, 118]. The other JLab data as well as all
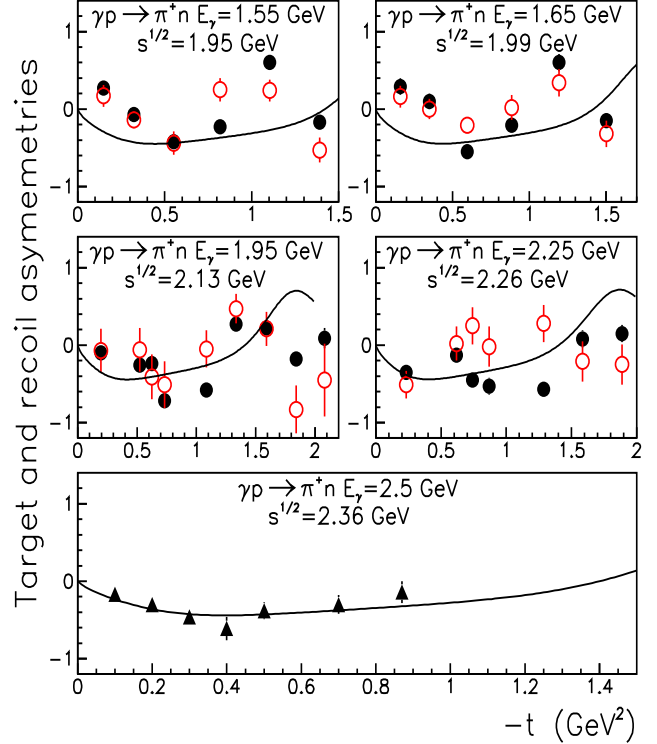
older experimental results for the higher $|t|$ region are simply beyond the applicability of our model.

Above $|t| \simeq 2$ GeV the data show first an almost t independent behavior and then increase sharply as $-t$ approaches its maximum value. The largest -t value corresponds to the smallest value of $|u|$, which is related to s and t by $s+t+u=2m_N^2+m_\pi^2$. It is known that the reaction mechanism at small $|u|$ and at small $|t|$ involves different exchanges. The reaction at small $|t|$ is dominated by the meson poles and cuts included in the Regge model constructed in this work. On the other hand, the rising cross sections at small $|u|$ (large $|t|$) observed in Fig. 11 are due to the exchange of baryon resonances.

In the central region $2 \leq -t \leq 5$ GeV^2 of Fig. 11, both $|t|$ and $|u|$ are large and hence the contributions from t- and u-channel exchanges become very small. The main feature of the cross sections in this middle region is that they are almost independent of t and hence are very unlikely due to nucleon resonances with reasonably narrow widths, *i.e.* with widths ≤ 300 MeV. The most plausible interpretation can be found from the point of view of perturbative QCD. The essential idea is that at large momentum transfer the basic interactions must be directly due to the quarks in the nucleon. As was proposed in Refs. [139, 140] the energy dependence of the reaction cross sections for this case is driven by the total number of elementary fields in the initial (n_i) and final (n_f) states. Following dimensional counting for the invariant amplitude $\mathcal{M}$ [141] the energy dependence of the differential cross section of the $n_i \to n_f$ transi-
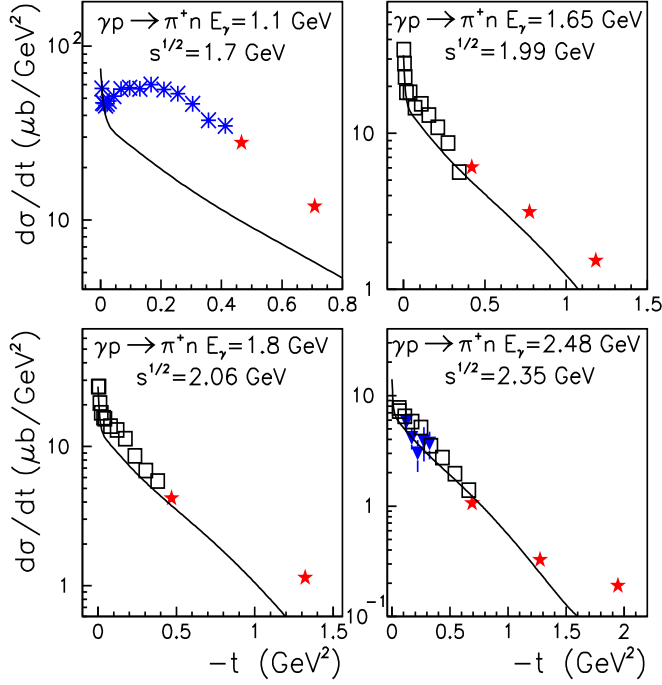
Fig. 10. The $\gamma p \rightarrow \pi^+ n$ differential cross section as a function of $-t$ at different photon energies E_γ. The data are taken from Refs. [115] (inverse close triangles), [113,114] (open squares) and [112] (asterisk). The stars are the experimental results from the JLab Hall A Collaboration [65]. The solid lines show results of our model calculation.
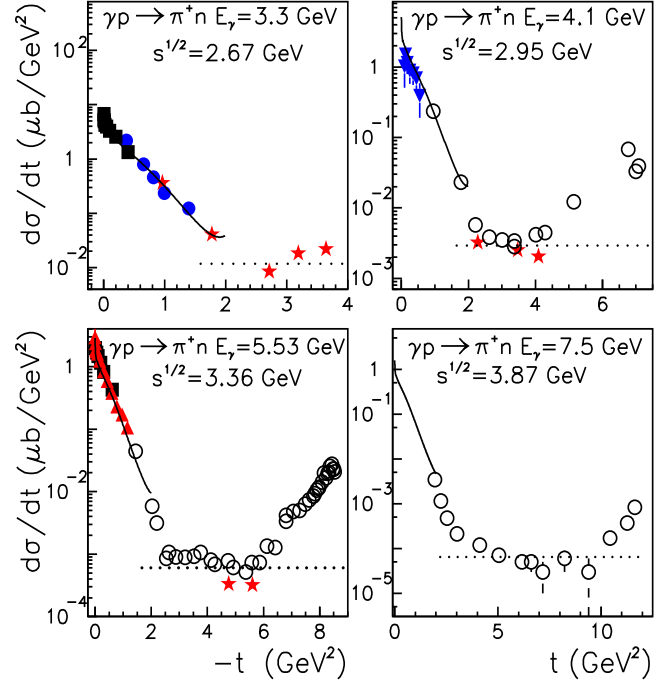
Fig. 11. The $\gamma p \rightarrow \pi^+ n$ differential cross section as a function of $-t$ at different photon energies E_γ. The data are taken from Refs. [116] (filled squares), [122] (filled triangles), [118] (filled circles) and [120, 121] (open circles). The stars are the experimental results from the JLab Hall A Collaboration [65]. The solid lines show our results based on the parameters listed in Table 3. The dotted lines are results obtained with Eq. (32).

tion is given as

$$\frac{d\sigma}{dt} = \frac{|\mathcal{M}|^2 F(t)}{16\pi(s-m_N^2)^2} \overset{m_N^2 \ll s}{=} \frac{s^{-(n_i-2)-(n_f-2)}F(t)}{16\pi s^2}$$
$$\propto s^{-7}F(t), \tag{32}$$

since for single pion photoproduction $n_i=4$ and $n_f=5$. Here $F(t)$ does not depend on s but accounts for the t-dependence of the hadronic wave functions and partonic scattering.

In order to see whether the data shown in Fig.11 follow the dimensional counting rule (also called the quark counting rule), we normalize the expression for $d\sigma/dt$ in Eq. (32) with $F(t) = 1$ to the data at $t=5$ GeV^2 and at $E_\gamma=7.5$ GeV, *i.e.* at the highest of the considered photon energies, and then use Eq. (32) to predict the cross sections at other energies. These predictions are shown by dotted lines in Fig. 11 and agree remarkably well with the data at all considered energies. It appears that the dimensional counting rule, as given in Eq. (32), is fulfilled very well. Such a conclusion was drawn also in Refs. [65,66] by analyzing the JLab data alone. It is an outstanding challenge to understand this smooth $t-$dependence. One possibility is to explore more rigorously the handbag mechanism [142,143], which yields a reasonable description of the π^+/π^- ratio.

4 Results for $\gamma n \rightarrow \pi^- p$

The strategy for the analysis of negative pion photoproduction is similar to that described in Section 3 for positive pions. Some

general information on the data on $\gamma n \rightarrow \pi^- p$ included in our global fit is listed in the Tables 6 and 7.

The measurement of the $\gamma n \rightarrow \pi^- p$ reaction can be only done with a deuteron target. The extraction of data for negative pion photoproduction from the deuteron reaction is based on the so-called spectator model, *i. e.* the single scattering impulse approximation. Thereby, it is assumed that the proton of the deuteron is the spectator and its role in the γn interaction is only due to the Fermi motion of the bound neutron. This is, in principle, a reliable method [144,145,146,147,148,149, 150,151] as long as one measures the momentum distribution of the proton and one takes only those events which fulfill the spectator condition, *i. e.* those events where the proton momentum is smaller than the momentum of the neutron. However, in practice often the spectator proton and the final neutron are not even identified. In that case one might expect [150] some discrepancies between the model calculations and the data as well as between different measurements. Some important details of the deuteron experiments will be given in the following in order to discuss possible reasons for the observed discrepancies.

4.1 Results at $E_\gamma \geq 3$ GeV

Fig. 12 shows differential cross sections for $\gamma n \rightarrow \pi^- p$ measured [116,118,155] at different photon energies together with

Table 6. The $\gamma n \to \pi^- p$ data on differential cross section analyzed in the present paper.

E_γ (GeV)	$\sqrt{s}$ (GeV)	$-t_{min}$ (GeV^2)	$-t_{max}$ (GeV^2)	Reference
		Differential cross section, $d\sigma/dt$		
1.1	1.7	0.41	1.11	[152]
1.1	1.7	0.41	1.11	[153]
1.1	1.7	4.2×10^{-3}	1.37	[152]
1.1	1.7	0.25	0.71	[65]
1.65	1.99	0.72	1.49	[152]
1.65	1.99	0.42	1.19	[65]
1.8	2.06	0.80	2.10	[152]
1.8	2.06	0.19	2.64	[154]
1.8	2.06	0.48	1.33	[65]
2.48	2.35	0.69	1.94	[65]
3.0	2.55	0.15	1.16	[118, 124]
3.32	2.67	0.96	3.64	[65]
3.4	2.69	0.37	1.39	[118, 124]
3.4	2.69	3.0×10^{-3}	0.4	[116]
4.15	2.95	1.25	3.47	[65]
5.0	3.2	6.8×10^{-3}	0.53	[116]
5.53	3.36	3.18	4.73	[65]
8.0	3.99	9.9×10^{-3}	0.89	[155]

Table 7. The $\gamma n \to \pi^- p$ data on the polarized photon asymmetry Σ (denoted formerly as A [92]) analyzed in the present paper.

| E_γ (GeV)	$\sqrt{s}$ (GeV)	$-t_{min}$ (GeV^2)	$-t_{max}$ (GeV^2)	Reference
		Polarized photon asymmetry Σ		
3.0	2.55	0.15	1.16	[124]
3.4	2.69	0.05	0.6	[133]
16.0	5.56	5.5×10^{-3}	1.19	[125]

results of our model calculation. Indeed, these are practically all π^- photoproduction data for $E_\gamma \geq 3$ GeV that are available in the literature.

Let us first provide some details on the above experiments which will be useful later in discussing the observed discrepancies between the older measurements and the most recent results from JLab reported by the Hall A Collaboration [65, 66]. In the experiment of Ref. [116] $\gamma d \to \pi^- 2p$, $\gamma d \to \pi^+ 2n$, and in addition $\gamma p \to \pi^+ n$ were studied in order to check the validity of the spectator model. The experiment was performed at DESY with a bremsstrahlung beam and by detecting only the pions with a magnetic spectrometer. At small $-t$ the relation between the photon energy and the pion momentum is almost identical to the one for photoproduction on a free nucleon. Thus by measuring the pion momentum at a given angle one can reconstruct the photon energy. The Fermi motion in the deuteron results in an uncertainty of ± 100 MeV in the invariant mass energy of the final system. Furthermore, utilizing simulation calculations of the reaction based on the Hulthén deuteron wave function it was found that the computed momentum spectrum of the pions is in good agreement with the measured one. The

energetic separation between single and multiple pion photoproduction was good enough to avoid di-pion contamination. Single pion photoproduction was studied by using the photon energy interval of 200 MeV around E_γ=3.4 GeV and 5 GeV.

We should also mention that in Ref. [116] it was observed that at $|t| \geq 0.3$ GeV^2 the differential cross sections for π^+-meson photoproduction on deuterium and hydrogen are almost identical, while at smaller momentum transfers they differ substantially, *i. e.* up to a factor of $\simeq 2$. That was qualitatively understood from spin and isospin restrictions of the spectator model [156]. A similar suppression of the π^+-meson yield from deuterium at small angles was observed in lower-energy experiments [157]. Furthermore, the π^-/π^+ ratio was evaluated under the assumption that the corrections for the $\gamma d \to \pi^- 2p$ and $\gamma d \to \pi^+ 2n$ reactions are the same.

The circles in Fig. 12 are data taken [118] at the Cambridge Electron Accelerator. The results at E_γ=3.4 GeV are published [118], while the data for the differential cross section at E_γ=3 GeV, mentioned in Ref. [124], are available from the Durham Data Base [109]. The $\gamma d \to \pi^- 2p$, $\gamma d \to \pi^+ 2n$ and $\gamma p \to \pi^+ n$ reactions were studied by detecting only the π^--meson. The reconstruction procedure for the reaction is almost identical to that applied in Ref. [116]. The energy of the incident photon was determined by a subtraction method and could be evaluated to an accuracy of ± 60 MeV in the considered range from 3 to 3.7 GeV (explored in the search for the $N^*(2645)$ baryon). Under the assumption that the spectator nucleon is at rest the missing mass for an interacting nucleon was reconstructed in order to separate single pion photoproduction from multiple pion contributions.
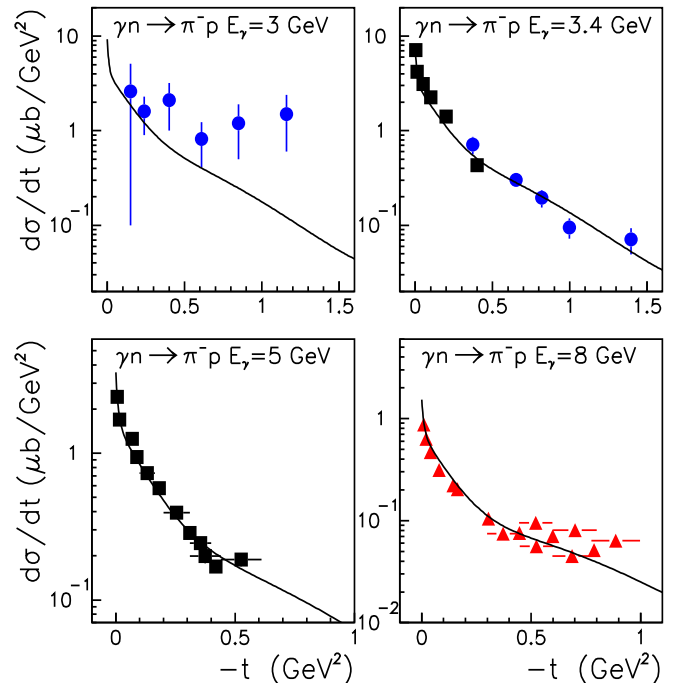
Fig. 12. The $\gamma n \to \pi^- p$ differential cross section as a function of $-t$ at different photon energies E_γ. The data are taken from Refs. [116] (filled squares), [118, 124] (filled circles), and [155] (filled triangles). The solid lines show results of our model calculation.
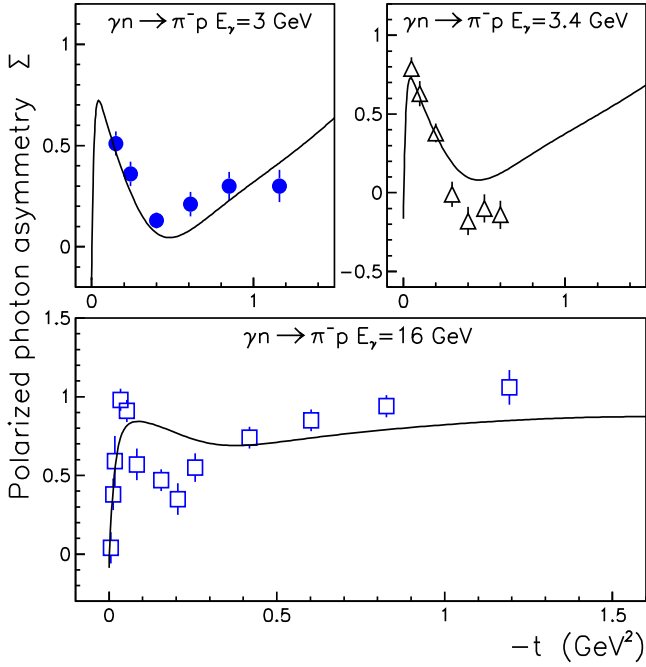
Fig. 13. Polarized photon asymmetry from $\gamma n \to \pi^- p$ reaction as a function of $-t$ at different photon energies, E_γ. The data are taken from Refs. [124] (filled circles), [125] (open squares) and [133] (open triangles). The solid lines show results of our model calculation.

Fig. 14. The $\gamma n \to \pi^- p$ differential cross section as a function of $-t$ at different photon energies E_γ. The data are taken from Refs. [153] (open circles), [152] (filled inverse triangles) and [154] (filled triangles). The stars are the experimental results from the JLab Hall A Collaboration [65]. The solid lines show our results based on the parameters listed in Table 3.

Our calculation reproduces the π^--meson data at E_γ=3.4 GeV rather well. The differential cross section at E_γ=3 GeV is described qualitatively. But it looks as if some additional contribution is required for the range of $-t \geq 0.4$ GeV^2, say, though one should keep in mind that the data at E_γ=3 GeV are afflicted by fairly large errors. In this context we want to recall that we reasonably reproduce the differential cross section and polarization data for positive pion photoproduction available around E_γ=3 GeV, cf. Figs. 1 and 3.

One could speculate that this deviation of the model result from the data is a signal for an excited baryon with mass around 2.55 GeV. For instance, the $N^*(2645)$ resonance was observed in pion-nuclear interactions [158,159] but was not detected in the photoproduction of positive and neutral pions. If the baryon is a member of a U-spin multiplet with U=3/2 it could not be excited in the interaction of photons with protons because the photon is considered to be U=0. In case of a neutron target both n and the neutral N^* have U=1 and the corresponding excitation is allowed [118,124]. It is worth mentioning that there is no obvious evidence for the presence of such a resonance in the polarized photon asymmetry shown in Fig. 13.

The data at E_γ=8 GeV were measured [155] at the Stanford Linear Accelerator. Again only pions were detected and the reaction was reconstructed by measuring the pion momentum distribution resulting from photons near the bremsstrahlung dip. It was emphasized that such a reconstruction of single pion photoproduction is quite reasonable at small $-t$ but becomes impractical at $|t| \geq 2$ GeV, unless the other final state particles are also detected. To test the spectator mechanism, $\gamma d \to \pi^+ 2n$ as well as $\gamma p \to \pi^+ n$ reactions were studied. It was found [155]
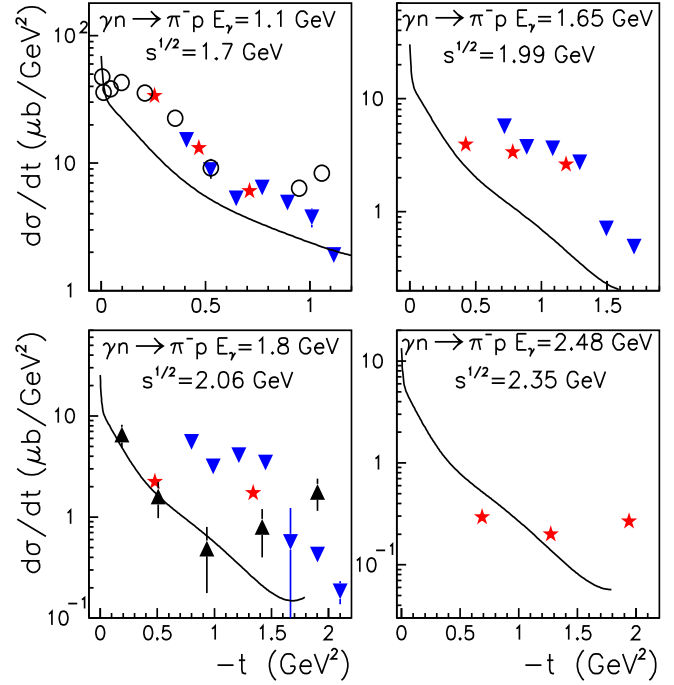
that at $|t|<0.5$ GeV^2 the differential cross sections for π^+-meson photoproduction on deuterium and hydrogen differ up to a factor of around 8. The reasons for such a discrepancy were investigated in detail and it was argued that the Pauli exclusion principle explains completely the observed effect. The relevant corrections were done for presenting the π^--meson photoproduction data. Fig. 12 clearly proofs that we perfectly reproduce the π^--meson photoproduction differential cross section at E_γ=8 GeV.

Finally, in Fig. 13 data on the polarized photon asymmetry for the reaction $\gamma n \to \pi^- p$ [124,125,133] at photon energies 3, 3.4 and 16 GeV are presented. In these experiments the reaction was reconstructed similar to the procedures described above. The model calculation describes the experimental results well – with exception of some data points.

4.2 Comparison with the JLab data

Differential cross sections for $\gamma n \to \pi^- p$ at photon energies between 1.1 GeV and 5.5 GeV were reported [65,66] recently by the Hall A Collaboration at JLab. Although most of the data were obtained for large $|t|$, at some photon energies the measurements extend to the region of $|t|<2$ GeV^2 and can be directly compared with our calculation.

We want to emphasize that this experiment with a deuterium target has some significant advantages as compared to the other measurements discussed in the previous subsection.

In particular, both the π^--meson and the proton were detected in coincidence. Based on two-body kinematics, the incident photon energy was reconstructed. That allows one to reconstruct the spectator momentum distribution which was found to be in good agreement with the Argonne, Paris and Bonn deuteron wave functions at momenta below 400 MeV/c.

The differential cross sections for $\gamma n \to \pi^- p$ are presented in Figs. 14 and 15 as a function of $-t$ for different photon energies. The measurements at JLab were done at $E_\gamma \simeq 1.1$, 1.65, 1.8, 2.48, 3.3, 4.1 and 5.53 GeV, which correspond to $\sqrt{s} \simeq 1.7$, 1.99, 2.06, 2.35, 2.67, 2.95 and 3.36 GeV, respectively. For completeness and for illustrating the compatibility with other available experimental results we also show differential cross sections from Refs. [116, 118, 153, 152] obtained at almost the same photon energies.

It is instructive to recall here the results of our analysis of the $\gamma p \to \pi^+ n$ data by the Hall A Collaboration [65, 66] at the same photon energies and the same range of t, shown in Figs. 10 and 11. There, we found that at $\sqrt{s}=1.7$ GeV our calculation substantially underestimates the π^+ spectrum and we observe a similar deficiency now for π^--meson photoproduction. This discrepancy is most likely associated with contributions from known resonances in that energy region which are missing in our model calculation. At the energies $\sqrt{s}=1.99$ and 2.06 GeV the positive photoproduction spectra at $|t|\leq 0.7$ GeV^2 is reasonably described by our model calculation, and for the energies 2.35 and 2.67 GeV even up to roughly $|t|=1.5$ GeV^2. (There are no experimental points at $|t|\leq 2$ GeV^2 for $\sqrt{s}=2.95$

and 3.36 GeV.) Interestingly, the situation for negative pion photoproduction is somewhat different. While the model reproduces the $\gamma n \to \pi^- p$ differential cross sections at $\sqrt{s}\simeq 2.67$ and 2.95 GeV quite well up to $|t|\approx 1.5$ GeV^2, we observe a much more substantial deviation at the lower energies and for $|t|\geq 0.7$ GeV^2. In particular, at $\sqrt{s}=1.99$, 2.06 and 2.35 GeV the t dependence of negative pion photoproduction differs drastically from that for positive pions for $|t|\geq 0.5$ GeV^2, say. In fact, within the range $0.5<|t|<2$ GeV^2 where the JLab data are available, the differential cross sections for $\gamma n \to \pi^- p$ are practically independent of the four-momentum transfer squared. Data from other experiments [152, 154] exhibit a comparable behavior although they are afflicted by large uncertainties. Note that a very similar t dependence was observed in negative pion photoproduction [118] at $E_\gamma=3$ GeV, or $\sqrt{s}=2.55$ GeV, presented in Fig. 12. This could be an indication for contributions from excited baryons with masses lying around $1.99\leq\sqrt{s}\leq 2.55$ GeV. The range seems to be too large for a single resonance, unless one assumes the contribution to be from a rather broad ($\simeq 600$ MeV) structure.

We note that the GWU PWA [87, 101, 160] reproduces nicely π^+ as well as π^--meson photoproduction data at $\sqrt{s}\leq 2.1$ GeV. In particular, it describes the flat t-dependence for negative pions. It is unlikely that U symmetry was implemented in this analysis and the most natural expectation is that the PWA of the data yields a much larger photon coupling to the neutron than to the proton for resonances located within the range of $1.99\leq\sqrt{s}\leq 2.55$ GeV. Indeed the SM-95 solution [87] finds evidence for the excited baryons $F_{35}(1905)$, $D_{35}(1930)$ and F_{37} (1950), but the results for the γn couplings are not given in the corresponding publication. In this context, let us mention that it was shown within the $1/N_c$ expansion, based on the approximate dynamical spin-flavour symmetry $SU(4)$ of QCD in the large N_c limit [161, 162], that the photoproduction on the neutron can be larger than that on the proton. Thus, it is conceivable that the chances for exciting a baryon in $\gamma n \to \pi^- p$ are substantially larger than in $\gamma p \to \pi^+ n$ or $\gamma p \to \pi^0 p$ reactions. Furthermore, according to the systematic study of Ref. [161] one should expect that such an excited baryon is a nucleon, because photo-excitation of Δ resonances should be identical for proton and neutron targets.

The presently available data are too scarce to allow us to draw a definitive conclusion. Apparently new precise measurements at $|t| < 2$ GeV^2 and photon energies $1.6\leq E_\gamma\leq 3.4$ GeV are required to clarify the situation. At such energies this t range is quite promising for baryon spectroscopy, because at large $-t$ the contribution from hard QCD processes might dominate the reaction.
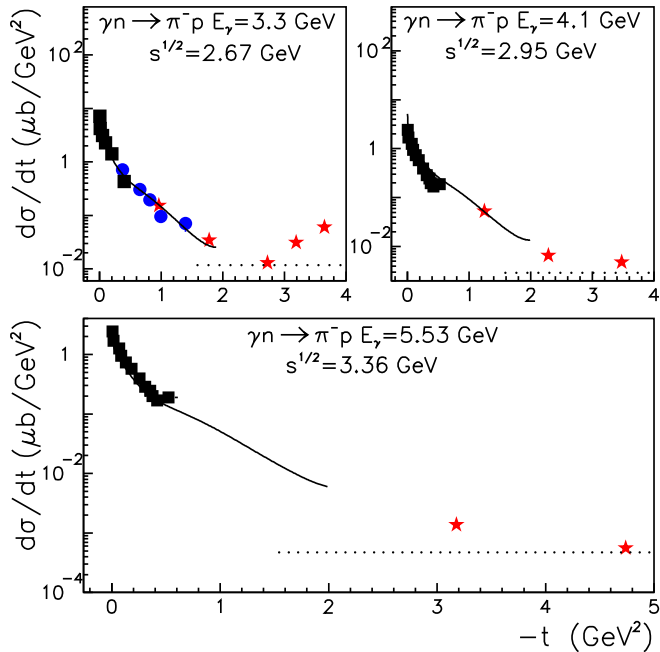

Fig. 15. The $\gamma n \to \pi^- p$ differential cross section as a function of $-t$ at different photon energies, E_γ. The data are taken from Refs. [118] (filled circles) and [116] (filled squares). The stars are the experimental results from the JLab Hall A Collaboration [65]. The solid lines show our results based on the parameters listed in Table 3. The dotted line shows result obtained by Eq. (32) and normalized to the $\gamma p \to \pi^+ n$ data as explained in the text.

5 The π^-/π^+ ratio

Quite interesting information on charged pion photoproduction is provided by the ratio $\mathcal{R}$ of the $\gamma n \to \pi^- p$ to $\gamma p \to \pi^+ n$ differential cross section as a function of t and the photon energy or $\sqrt{s}$. Since at small $|t|$ ($|t|\leq m_\pi^2$) single pion photoproduction is dominated by t-channel pion exchange, it follows that $\mathcal{R}=1$ – independent of the energy. At moderate t the interference between the π and ρ exchanges is expected to result in

a decrease of $\mathcal{R}$ as $|t|$ increases, following Eq. (1). With further increase of $|t|$ the contribution of pion exchange vanishes and ρ exchange dominates so that one might expect a return to $\mathcal{R}=1$. However, since other contributions, summarized in Table 1, could be sizeable the evolution of $\mathcal{R}$ with t is not trivial. Thus, this evolution directly reflects the presence of contributions to the reaction amplitude from exchanges with different quantum numbers.

Note that the π^-/π^+ ratio at large $|t|$ can be compared with the handbag calculations [163, 142, 143] based on hard gluon exchange. Therefore, it is important to inspect the behavior of $\mathcal{R}$ when approaching $-t\simeq2$ GeV^2. Here one expects the transition between perturbative QCD as modelled by Regge theory and hard QCD processes.

Figure 16 shows the ratio $\mathcal{R}$ of the $\gamma n\to\pi^- p$ to $\gamma p\to\pi^+ n$ differential cross section as a function of the four-momentum transfer squared. Here we include data for photon energies $3.4\le E_\gamma \le16$ GeV. In each of the experiments [125, 116, 118, 155] the ratio $\mathcal{R}$ was measured for a fixed photon energy as a function of t or of the pion production angle, θ^*. The data exhibit a very specific t-dependence, that is almost independent of the energy. Approaching $t = 0$ the ratio $\mathcal{R}$ is close to 1, as expected from the dominance of pion exchange at $|t|\le m_\pi^2$. Then the ratio decreases because of the interplay between the various contributions to the photoproduction amplitude listed in Table 1 and entering Eq. (1). However, with increasing $|t|$ the ratio does not converge to unity as one might expect from the dominance of ρ exchange. This clearly indicates that with increasing $-t$ the reaction is still governed by contributions from several different processes and that one will not able to reproduce such a t dependence within a simple $\pi+\rho$ model.
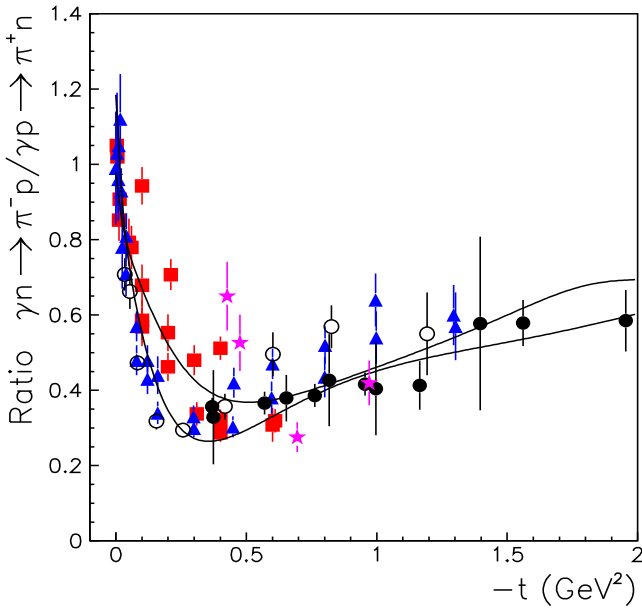

Fig. 17. The ratio of the $\gamma n\to\pi^- p$ to $\gamma p\to\pi^+ n$ differential cross section as a function of invariant collision energy shown for different intervals of the four-momentum transfer squared. The filled circles are experimental results from Refs. [116, 125, 118, 155], while the stars indicate data from JLab [65, 66]. The bands show the variation of $\mathcal{R}$ within the indicated range of t as predicted by our model.

Fig. 16. The ratio of the $\gamma n\to\pi^- p$ to $\gamma p\to\pi^+ n$ differential cross section as a function of $-t$. The data for $3.4\le E_\gamma \le16$ GeV are taken from Refs. [116] (filled squares), [125] (open circles), [118] (filled circles) and [155] (filled triangles). The two solid lines show our results obtained for E_γ=3.4 and 16 GeV.
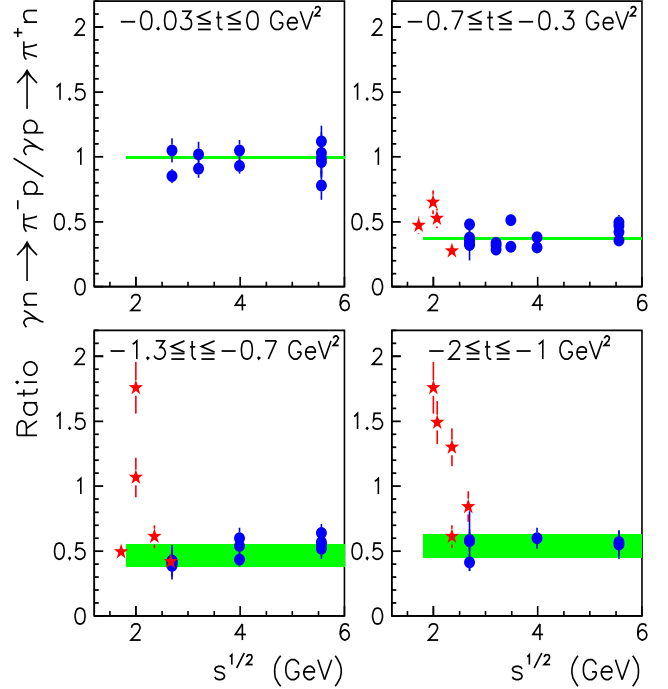
The π^-/π^+ ratio was also measured recently at JLab by the Hall A Collaboration [65, 66]. As mentioned above, this experiment was motivated by hard QCD physics [139, 140] and devoted to pion photoproduction at large $|t|$. Although it is difficult to provide an estimate for the absolute value of the reaction cross section within QCD inspired models, predictions for the π^-/π^+ ratio and for some polarization observables at large $|t|$ can be made with more confidence [142, 143, 163]. Indeed, the calculations of Refs. [142, 143] reproduce $\mathcal{R}$ at large $-t$ rather well. Part of the data were also taken for $|t|<2$ GeV^2, which allows us to compare those data with our calculation and to search for a signature [139, 140, 142, 143] of the transition from pQCD, modelled by Regge theory, to hard QCD.

On the other hand, the JLab experiment [65, 66] was done at different photon energies and for fixed angles θ^* in the overall cm system, which complicates the comparison with other results. Specifically, it is not possible to evaluate the t dependence of the π^-/π^+ ratio from these data and compare it with either that of the other data sets or of our model.

The solid lines in Fig. 16 show our results for E_γ=3.4 and 16 GeV. The model reproduces the t dependence qualitatively and exhibits only a mild dependence on energy. Note that within this energy range the differential cross section itself changes by almost two orders of magnitude, as is visible in Figs. 1 and 2.

In any case, we can directly test the model by considering the $\sqrt{s}$ dependence of the ratio $\mathcal{R}$ at fixed values of t. Since the data are not available at exactly the same t one can select appropriate ranges. This is done in Fig. 17, where we display

the dependence of $\mathcal{R}$ on the invariant collision energy $\sqrt{s}$ for different intervals of t. The band indicates the variation of $\mathcal{R}$ as predicted by the model for the selected range of t.

Obviously the π^-/π^+ ratio obtained from experimental results available at $-0.03 \leq t \leq 0$ GeV^2 is close to unity at energies $2.7 \leq \sqrt{s} \leq 5.6$ GeV. That is exactly what one would expect from the pion exchange dominance at $|t| \leq m_\pi^2$. This feature is reproduced by the model. With regard to other intervals of t which we have considered, the data above $\sqrt{s} \simeq 2.5$ GeV from Refs. [125, 116, 118, 155] are well described by our model. Furthermore, the JLab data [65, 66] available at the same energies are in good agreement with other data and also with our calculation. However, in the range $1.7 \leq \sqrt{s} \leq 2.5$ GeV, the ratio of the $\gamma n \rightarrow \pi^- p$ to $\gamma p \rightarrow \pi^+ n$ differential cross section shows a clear resonance-like structure, which is most prominently noticeable at $0.7 \leq |t| \leq 2$ GeV^2. This observation is consistent with the conclusions we drew from our analysis of the π^- differential cross section above.

6 Conclusion

We analyzed the data on charged pion photoproduction available at photon energies $3 \leq E_\gamma \leq 8$ GeV and at four-momentum transfer squared $|t| \leq 2$ GeV^2 within the Regge approach. The model was constructed by taking into account both pole and cut exchange t-channel helicity amplitudes. We consider the b_1, ρ and a_2 trajectories and pion exchange and fix the unknown model parameters such as the helicity couplings by fitting experimental results on differential cross sections, the polarized photon asymmetry and recoil and target asymmetries.

The model provides a reasonable description of the data, indicating that for the energy range considered single pion photoproduction is dominated by nonresonant contributions. The calculation was extended to lower photon energies in order to examine the data with regard to possible signals for the excitation of baryonic resonances with masses between 2 and 3 GeV. We detected a systematic discrepancy between the calculation and the data on $\gamma n \rightarrow \pi^- p$ differential cross sections for photon energies from 1.65 to 3 GeV (invariant collision energies of $1.99 \leq \sqrt{s} \leq 2.55$ GeV) in the region $-t \geq 0.5$ GeV^2. The model results for $\gamma p \rightarrow \pi^+ n$ also show deviations from the data in this energy and t region, though here the disagreement is less pronounced.

The differential cross sections for $\gamma n \rightarrow \pi^- p$ which are at variance with the model calculation are those measured at ELSA (Bonn) [152] and very recently at JLab [66]. Unfortunately, the amount and accuracy of the experimental results in the relevant energy region is still insufficient for a more detailed quantitative analysis and for the evaluation of possible contributions from the excitation of high-mass baryons. Nevertheless, we observe a resonance-like structure in the ratio of the $\gamma n \rightarrow \pi^- p$ to $\gamma p \rightarrow \pi^+ n$ differential cross sections taken at fixed intervals of t and shown as a function of $\sqrt{s}$. This ratio exhibits a noticeable enhancement at $1.7 \leq \sqrt{s} \leq 2.5$ GeV as compared to lower and higher energies.

Our findings suggest that the prospects for the excitation of baryon resonances on neutrons via photons could be substantially larger than on protons. If this is the case, it will be more difficult to observe such resonance excitations in the $\gamma p \rightarrow \pi^0 p$

reaction. Evidently, the validity of this conjecture can be examined via the analysis of data reported very recently [164] by the CB-Collaboration at ELSA. Note that in the framework of the $1/N_c$ expansion based on the approximate dynamical spin-flavour symmetry, $SU(4)$, of QCD in the large N_c limit, it was shown [161, 162] that photoproduction on the neutron can be very different from that on the proton. Furthermore, according to the systematic study of Ref. [161] one might expect that such an excited baryon is a nucleon, because photo-excitation of Δ resonances is identical for proton and neutron targets.

Further progress in understanding the observed discrepancies requires new dedicated experiments on the $\gamma n \rightarrow \pi^- p$ and $\gamma n \rightarrow \pi^0 n$ reactions at photon energies $1.6 \leq E_\gamma \leq 3$ GeV. Apparently polarization measurements are necessary to enable a reconstruction of the quantum numbers of the excited baryons.

References

1. N. Isgur and G. Karl, Phys. Rev. D **18**, 4187 (1978) .
2. S. Capstick and N. Isgur, Phys. Rev. D **34**, 2809 (1986).
3. S. Capstick and W. Roberts, Phys. Rev. D **47**, 1994 (1993).
4. S. Capstick and W. Roberts, Phys. Rev. D **49**, 4570 (1994) [arXiv:nucl-th/9310030] .
5. M.A. Shifman, A.I. Vainshtein and V.I. Zakharov, Nucl. Phys. B **147**, 385 (1979).
6. B.L. Ioffe, Nucl. Phys. B **188**, 317 (1981).
7. Ulf-G. Meißner, *Encyclopedia of Analytic QCD*, ed. M. Shifman, World Scientific [arXiv:hep-ph/0007092].
8. B.L. Ioffe, Prog. Part. Nucl. Phys. **56**, 232 (2006) [arXiv:hep-ph/0502148].
9. M. Gell-Mann and M. Levy, Nuovo Cim. **16**, 705 (1960).
10. Y. Nambu and G. Jona-Lasino, Phys. Rev. **122**, 345 (1961).
11. V. Barger and D. Cline, Phys. Rev. Lett. **16**, 913 (1966).
12. V. Barger and M. Olsson, Phys. Rev. **151**, 1123 (1966).
13. P.D.B. Collins, *Regge Theory and High Energy Physics*, Cambridge, Cambridge University Press (1977).
14. Y. Iwasaki, Prog. Theor. Phys. **44**, 777 (1970) .
15. F. Iachello, Phys. Rev. Lett. **63**, 1891 (1989).
16. D. Robson, Phys. Rev. Lett. **63**, 1890 (1989).
17. M. Kirchbach, Mod. Phys. Lett. A **12**, 3177 (1997) [arXiv:nucl-th/9712072].
18. M. Kirchbach, Int. J. Mod. Phys. A **15**, 1435 (2000) [arXiv:nucl-th/0007022].
19. J. C. Collins, A. Duncan and S. D. Joglekar, Phys. Rev. D **16**, 438 (1977).
20. X. D. Ji, Phys. Rev. Lett. **74**, 1071 (1995) [arXiv:hep-ph/9410274].

21. W.-M. Yao *et al.*, J. Phys. G **33**, 1 (2006).
22. L.Y. Glozman, Phys. Rept. **444**, 1 (2007) [arXiv:hep-ph/0701081].
23. L.Y. Glozman, Phys. Lett. B **475**, 329 (2000) [arXiv:hep-ph/9908207].
24. D. Jido, T. Hatsuda and T. Kunihiro, Phys. Rev. Lett. **84**, 3252 (2000) [arXiv:hep-ph/9910375].
25. D. Jido, M. Oka and A.Hosaka, Prog. Theor. Phys. **106**, 873 (2001) [arXiv:hep-ph/0110005].
26. T.D. Cohen and L.Y. Glozman, Phys. Rev. D **65**, 016006 (2002) [arXiv:hep-ph/0102206].
27. T.D. Cohen and L.Y. Glozman, Int. J. Mod. Phys. A **17**, 1327 (2002) [arXiv:hep-ph/0201242].
28. T.D. Cohen, Nucl. Phys. A **775**, 89 (2006) [arXiv:hep-ph/0605206].
29. R.L. Jaffe, D. Pirjol and A. Scardicchio, Phys. Rev. Lett. **96** 121601 (2006) [arXiv:hep-ph/0511081].
30. R.L. Jaffe, D. Pirjol and A. Scardicchio, Phys. Rept. **435** , 157 (2006) [arXiv:hep-ph/0602010].
31. P. Gonzalez, J. Vijande, A. Valcarce, and H. Garcilazo, Eur. Phys. J. A **31**, 515 (2007) [arXiv:hep-ph/0610257].
32. U. Löring, B. C. Metsch and H. R. Petry, Eur. Phys. J. A **10**, 395 (2001) [arXiv:hep-ph/0103289].
33. U. Löring, B. C. Metsch and H. R. Petry, Eur. Phys. J. A **10**, 447 (2001) [arXiv:hep-ph/0103290].
34. U. Löring and B. Metsch, arXiv:hep-ph/0110412.
35. G. Höhler, πN Newsletter **9**, 1 (1993).
36. G. Höhler, Landolt-Börnstein **9**, Springer, Berlin, 1983.
37. R. Koch, Nucl. Phys. A **448**, 707 (1986).
38. R. E. Cutkovsky *et al.*, Phys. Rev. D **20**, 2839 (1980).
39. A.W. Hendry, Phys. Rev. Lett. **41**, 222 (1978).
40. D. M. Manley and E. M. Saleski, Phys. Rev. D **45**, 4002 (1992).
41. R.A. Arndt, W.J. Briscoe, I.I. Strakovsky and R.L. Workman. Phys. Rev. C **74**, 045205 (2006) [arXiv:nucl-th/0605082].
42. SAID Partial Wave Analyis; the current solution is available on the web: http://gwdac.phys.gwu.edu/.
43. T.-S. H. Lee and L. C. Smith, J. Phys. G **34**, S83 (2007) [arXiv:nucl-th/0611034].
44. O. Krehl, C. Hanhart, S. Krewald and J. Speth, Phys. Rev. C **62**, 025207 (2000) [arXiv:nucl-th/9911080].
45. A. M. Gasparyan, J. Haidenbauer, C. Hanhart and J. Speth, Phys. Rev. C **68**, 045207 (2003) [arXiv:nucl-th/0307072].
46. S. N. Yang, G. Y. Chen and S. S. Kamalov, Nucl. Phys. A **790**, 229 (2007) [arXiv:nucl-th/0610076].
47. G. Y. Chen, S. S. Kamalov, S. N. Yang, D. Drechsel and L. Tiator, arXiv:nucl-th/0703096.
48. B. Juliá-Diaz, T.-S. H. Lee, A. Matsuyama, and T. Sato, arXiv:0704.1615 [nucl-th].
49. Y. Surya and F. Gross, Phys. Rev. C **53**, 2422 (1996).
50. T. Sato and T.S.H. Lee, Phys. Rev. C **54**, 2660 (1996) [arXiv:nucl-th/9606009].
51. M.G. Fuda and H. Alharbi, Phys. Rev. C **68**, 064002 (2003).
52. V. Pascalutsa and J. A. Tjon, Phys. Rev. C **70**, 035209 (2004) [arXiv:nucl-th/0407068].
53. H. Haberzettl, K. Nakayama and S. Krewald, Phys. Rev. C **74**, 045202 (2006) [arXiv:nucl-th/0605059].
54. A. Matsuyama, T. Sato, T.- S. H. Lee, Phys. Rept. **439**, 193 (2007) [arXiv:nucl-th/0608051].
55. T. Feuster and U. Mosel, Phys. Rev. C **59**, 460 (1999) [arXiv:nucl-th/9803057].
56. G. Penner and U. Mosel, Phys. Rev. C **66**, 055211 (2002) [arXiv:nucl-th/0207066].

57. A. Anisovich, E. Klempt, A. Sarantsev and U. Thoma, Eur. Phys. J. A **24**, 111 (2005) [arXiv:hep-ph/0407211].
58. A. V. Anisovich, A. Sarantsev, O. Bartholomy, E. Klempt, V. A. Nikonov and U. Thoma, Eur. Phys. J. A **25**, 427 (2005) [arXiv:hep-ex/0506010].
59. M.L. Perl, *High Energy Hadron Physics*, New York, Wiley (1974) 395.
60. P.D.B. Collins, *An Introduction to Regge Theory and High Energy Physics*, Cambridge University, Cambridge, England (1977) 275.
61. P.D.B. Collins and A.D. Martin, Rept. Prog. Phys. **45**, 335 (1982).
62. L. Caneschi, *Regge Theory of Low p_t Hadronic Interactions* Amsterdam, North-Holland (1989)
63. G. Matthiae, Rep. Prog. Phys. **57**, 743 (1994).
64. E. Levin, arXiv:hep-ph/9710546.
65. L. Y. Zhu *et al.*, Phys. Rev. C **71**, 044603 (2005) [arXiv:nucl-ex/0409018].
66. L. Y. Zhu *et al.*, Phys. Rev. Lett. **91**, 022003 (2003) [arXiv:nucl-ex/0211009]
67. M. Rahnama and J. K. Storrow, J. Phys. G **17**, 243 (1991).
68. J. Storrow, *Electromagnetic Interactions of Hadrons*, ed. A. Donnache and G. Shaw, **1**, New York Plenum (1978).
69. B. H. Kellett, Nucl. Phys. B **25**, 205 (1970).
70. J.S. Ball, W.R. Frazer and M. Jacob, Phys. Rev. Lett. **20**, 518 (1968).
71. F. Henyey, Phys. Rev. **170**, 1619 (1968).
72. J. S. Ball, H. W. Müller and B. K. Pal, Phys. Rev. D **4**, 2065 (1971).
73. J. D. Jackson and C. Quigg, Phys. Lett. B **29**, 236 (1969).
74. J. D. Jackson and C. Quigg, Phys. Lett. B **33**, 444 (1970).
75. J. Froyland and D. Gordon, Phys. Rev. **177**, 2500 (1969).
76. M. Rahnama and J. K. Storrow, J. Phys. G. **8**, 455 (1982).
77. M. Guidal, J.M. Laget and M. Vanderhaeghen, Nucl. Phys. A **627**, 645 (1997).
78. M. Vanderhaeghen, M. Guidal and J.M. Laget, Phys. Rev. C **57**, 1454 (1998).
79. N. Dombey, Nuovo Cim. **32**, 1696 (1964).
80. N. Dombey, Phys. Lett. B **30**, 646 (1964).
81. B. H. Kellett, Nucl. Phys. B **35**, 517 (1971).
82. M. L. Blackmon, G. Kramer and K. Schilling, Nucl. Phys. B **12**, 495 .(1969)
83. G. Kramer and P. Stichel, Z. Phys. **178**, 519 (1964).
84. F.A. Berends, Phys. Rev. D **1**, 2590 (1970).
85. F.A. Berends and G.B. West, Phys. Rev. **188**, 2538 (1969).
86. R. Dolen, D. Horn and C. Schmid, Phys. Rev. **166**, 1768 (1968).
87. R. A. Arndt, I. I. Strakovsky and R. L. Workman, Phys. Rev. **C 53** (1996) 430; updates available on the web: http://gwdac.phys.gwu.edu/
88. A. C. Irving and R. P. Worden, Phys. Rept. **34**, 117 (1977).
89. N.J. Sopkovitch, Nuovo Cim. **26**, 186 (1962).
90. K. Gottfried and J.D. Jackson, Nuovo Cim. **34**, 735 (1964).
91. J.D. Jackson, Rev. Mod. Phys. **42**, 12 (1970).
92. R. Worden, Nucl. Phys. B **37**, 253 (1972).
93. R.C. Arnold, Phys. Rev. **153**, 1523 (1967).
94. V.M. Gribov, I.Y. Pomeranchuk and K.A. Ter-Martirosyan, Phys. Rev. **139B**, 184 (1965).
95. A.R. White, Nucl. Phys. B **50**, 93 (1972).
96. A.R. White, Nucl. Phys. B **50**, 130 (1972).
97. G. F. Chew, M. L. Goldberger, F. E. Low and Y. Nambu, Phys. Rev. **106**, 1345 (1957).
98. B.H. Wiik, Proc. Int. Symp. on Electron and Photon Interactions at High Energies, Ithaca, New York, Aug 1971, 163.
99. I. S Barker, A. Donnachie and J. K. Storrow, Nucl. Phys. B **95**, 347 (1975).

100. F. A. Berends, A. Donnachie and D. L. Weaver, Nucl. Phys. B **4**, 1 (1967).

101. R. A. Arndt, R. L. Workman, Z. Li and L. D. Roper, Phys. Rev. C **42**, 1853 (1990) .

102. C.B. Chiu and S. Matsuda, Phys. Lett. B **31**, 455 (1970).

103. A. Sibirtsev, K. Tsushima and S. Krewald, Phys. Rev. C **67**, 055201 (2003) [arXiv:nucl-th/0301015].

104. J. N. J. White, Phys. Lett. B **26**, 461 (1968).

105. J. N. J. White, Nucl. Phys. B **13**, 139 (1969).

106. F. Henyey, G. L. Kane, Jon Pumplin and M. H. Ross, Phys. Rev. **182**, 1579 (1969).

107. G. Kramer, K. Shilling and L. Stodolsky, Nucl. Phys. B **5**, 317 (1968).

108. N. Dombey, Phys. Lett. B **30**, 646 (1969).

109. The Durham High Energy Physics Databases; the data are available on the web: http: //durpdg.dur.ac.uk/HEPDATA/.

110. M. Rahnama and J. K. Storrow, Z. Phys. C **10**, 263 (1981).

111. I. S Barker, A. Donnachie and J. K. Storrow, Nucl. Phys. B **79**, 431 (1974).

112. S. D. Ecklund and R. L. Walker, Phys. Rev. **159**, 1195 (1967).

113. G. Buschhorn *et al.*, Phys. Rev. Lett. **17**, 1027 (1966).

114. G. Buschhorn *et al.*, Phys. Rev. Lett. **18**, 571 (1967).

115. J. P. Dowd, D. O. Caldwell, K. Heinloth and T. R. Sherwood, Phys. Rev. Lett. **18**, 414 (1967) .

116. P. Heide, U. Kötz, R. A. Lewis, P. Schmüser, H. J. Skronn and H. Wahl, Phys. Rev. Lett. **21**, 248 (1968).

117. P. M. Joseph, N. Hicks, L. Litt, F. M. Pipkin and J. J. Russell, Phys. Rev. Lett. **19**, 1206 (1967).

118. Z. Bar-Yam *et al.*, Phys. Rev. Lett. **19**, 40 (1967).

119. V. B. Elings *et al.*, Phys. Rev. **156**, 1433 (1967).

120. R. L. Anderson *et al.*, Phys. Rev. D **14**, 679 (1976).

121. R. L. Anderson *et al.*, Phys. Rev. Lett. **23**, 721 (1969).

122. A. M. Boyarski *et al.*, Phys. Rev. Lett. **20**, 300 (1968).

123. C. Geweniger *et al.*, Phys. Lett B **29**, 41 (1969).

124. Z. Bar-Yam *et al.*, Phys. Rev. Lett. **25**, 1053 (1970).

125. D. J. Sherden *et al.*, Phys. Rev. Lett. **30**, 1230 (1973).

126. P.J. Bussey *et al.*, Nucl. Phys. B **154**, 492 (1979).

127. H. Bienlein *et al.*, Phys. Lett. B **46**, 131 (1973).

128. P.S.L. Booth *et al.*, Phys. Lett. B **38**, 339 (1972).

129. M. Deutsch, L. Golub, P. Kijewski, D. Potter, D.J. Quinn and J. Rutherfoord, Phys. Rev. Lett. **29**, 1752 (1972).

130. H. Genzel *et al.*, Nucl. Phys. B **92**, 196 (1975).

131. C. C. Morehouse *et al.*, Phys. Rev. Lett. **25**, 835 (1970) .

132. P.J. Bussey *et al.*, Nucl. Phys. B **154**, 205 (1979).

133. H. Burfeindt *et al.*, Phys. Lett. B **33**, 509 (1970).

134. P. Stichel, Z. Phys. **180**, 170 (1964).

135. F. Ravndal, Phys. Rev. D **2**, 1278 (1970).

136. R. P. Bajpai, Nucl. Phys. B **26**, 231 (1971).

137. R. A. Arndt *et al.*, Phys. Rev. D **43**, 2131 (1991).

138. M. Batinić *et al.*, Phys. Rev. C **51**, 2310 (1995) [arXiv:nucl-th/9501011].

139. S. J. Brodsky and G. R. Farrar, Phys. Rev. Lett. **31**, 1153 (1973).

140. V.A. Matveev, R.M. Muradian and A.N. Tavkhelidze, Lett. Nuovo Cim. **7**, 719 (1973).

141. E. Byckling and K. Kajantie, Particle Kinematics, *ed. John Wiley and Sons, 1973*.

142. H.W. Huang and P. Kroll, Eur. Phys. J. C **17**, 423 (2000) [arXiv:hep-ph/0005318]

143. H.W. Huang, R. Jakob, P. Kroll and K. Passek-Kumericki, Eur. Phys. J. C **33**, 91 (2004) [arXiv:hep-ph/0309071].

144. H.O. Meyer and J. Niskanen, Phys. Rev. C **47**, 2474 (1993).

145. F. Duncan *et al.*, Phys. Rev. Lett. **80**, 4390 (1998).

146. H. Hann *et al.*, Phys. Rev. Lett. **82**, 2258 (1999).

147. H. Calén *et al.*, Phys. Rev. C **58**, 2667 (1998).

148. J. Zlomanczuk, *AIP Conf. Proc.* **603**, 211 (2001).

149. P. Moskal, arXiv:hep-ph/0408162.

150. A. Sibirtsev, J. Haidenbauer, S. Krewald and Ulf-G. Meißner, J. Phys. G **32**, R395 (2006) [arXiv:nucl-th/0608028].

151. M. Abdel-Bary et al., Eur. Phys. J. A **29**, 353 (2006).

152. H. J. Besch, F. Krautschneider, K. P. Sternemann and W. Vollrath, Z. Phys. C **16**, 1 (1982).

153. P. E. Scheffler and P. L. Walden, Nucl. Phys. B **75** 125 (1974).

154. P. Benz *et al.*, Nucl. Phys. B **65**, 158 (1973).

155. A. M. Boyarski *et al.*, Phys. Rev. Lett. **21**, 1767 (1968).

156. A. Baldin, Nuovo Cim. **8**, 569 (1958).

157. G. Neugebauer, W. Wales and R.L. Walker, Phys. Rev. **119**, 1726 (1960).

158. M.A. Wahlig *et al.*, Phys. Rev. Lett. **13**, 103 (1964).

159. A. Citron *et al.*, Phys. Rev. Lett. **13**, 205 (1964).

160. Z. Li, R. A. Arndt, L. D. Roper and R. L. Workman, Phys. Rev. C **47**, 2759 (1993) .

161. J.L. Goity and N.N. Scoccola, arXiv:hep-ph/0701244.

162. J.L. Goity and N.N. Scoccola, Phys. Rev. D **72** 034024 (2005) [arXiv:hep-ph/0504101].

163. A. Afanasev, C.E. Carlson and C. Wahlquist, Phys. Lett. B **398**, 393 (1997).

164. H. van Pee *et al.*, Eur. Phys. J. A **31**, 61 (2007) [arXiv:nucl-ex/07041776].